ESTIMATION OF ACTUAL EVAPOTRANSPIRATION USING MAPPING EVAPOTRANSPIRATION AT HIGH RESOLUTION USING INTERNALIZED CALIBRATION (METRIC) MODEL UNDER VARIABLE CLIMATIC CONDITIONS IN PESHAWAR BASIN, PAKISTAN

By

Sundas Gill Kiyani

NUST201261095MSCEE62512F

A thesis submitted in partial fulfillment of the requirements for the degree of Master of Science in GIS and Remote Sensing

Institute of Geographical Information Systems

School of Civil and Environmental Engineering

National University of Sciences & Technology

Islamabad, Pakistan

August 2014

CERTIFICATE

Certified that the contents and form of thesis entitled **"Estimation of Actual Evapotranspiration using Mapping Evapotranspiration at High Resolution using Internalized Calibration (METRIC) model under Variable Climatic Conditions in Peshawar basin, Pakistan"** submitted by Ms. Sundas Gill Kiyani has been found satisfactory for the requirement of Master of Science degree in Remote Sensing and Geographical Information Systems.

Supervisor: _____

Dr. Ejaz Hussain

Associate Dean, IGIS, NUST

Member: _____

Dr. Salman Atif

Assistant Professor**,**

IGIS, SCEE, NUST

Member: _____

Dr. Hamza Farooq Gabriel

Associate Professor,

NICE, SCEE, NUST

Member: _____

Ms. Khunsa Fatima

Lecturer,

IGIS, SCEE, NUST

ACADEMIC THESIS: DECLARATION OF AUTHORSHIP

I, Sundas Gill Kiyani, declare that this thesis and the work presented in it are my own and have been generated by me as the result of my own original research.

"Estimation of Actual Evapotranspiration using Mapping Evapotranspiration at High Resolution using Internalized Calibration (METRIC) model under Variable Climatic Conditions in Peshawar basin, Pakistan"

I conform that:

1. This work was done wholly by me in candidature for an MS research degree at the National University of Sciences and Technology, Islamabad.

2. Wherever I have consulted the published work of others, it has been clearly attributed.

3. Wherever I have quoted from the work of others, the source has been always cited. With the exception of such quotations, this thesis is entirely my own.

4. I have acknowledged all main sources of help.

5. Where the work of thesis is based on work done by myself jointly with others, I have made clear exactly what was done by others and what I have contributed myself.

6. None of this work has been published before submission. This work is not plagiarized under the HEC plagiarism policy.

Signed: ……………………

Date: ……………………..

DEDICATION

For my beloved family whose hard work and prayers have made me capable of facing troubles in life. They always stood by me and provided moral support and encouragement.

ACKNOWLEDGEMENTS

At last, I would also thank my institution National University of Sciences and Technology, without whom this project would have been a distant reality.

CONTENTS

LIST OF FIGURES

LIST OF TABLES

LIST OF NOTATIONS

Notation	Explanation
c_p	Air Specific Heat
d_r	Inverse Squared Relative Earth-Sun Distance
e_a	Actual Vapour Pressure
$ESUN_\lambda$	Solar Exo-Atmospheric Irradiance
f_c	Fractional Cover
K_c	Crop coefficient
K_p	Pan coefficient
L_λ	Spectral Radiance
r_{ah}	Aerodynamic Resistance
$R_{L\uparrow}$	Outgoing Longwave Radiation
$R_{L\downarrow}$	Incoming Longwave Radiation
R_n	Net Radiation
$R_{S\downarrow}$	Incoming Shortwave Radiation
α	Surface Albedo
ε	Surface Emissivity
θ	Solar Incidence Angle
Λ	Latent Heat of Vaporization
ρ_{air}	Air Density
ρ_λ	Reflectivity
σ	Stephen Boltzmann Constant
τ_{sw}	Atmospheric Transmissivity

LIST OF ABBREVIATIONS

Abbreviation	Representation
ASTER	Advanced Spaceborne Thermal Emission and Reflection Radiometer
AVHRR	Advanced Very High Resolution Radiometer
DEM	Digital Elevation Model
DN	Digital Number
ET	Evapotranspiration
ET_a	Actual Evapotranspiration
ET_{inst}	Instantaneous Evapotranspiration
ET_r	Reference Evapotranspiration
ET_rF	Reference Evapotranspiration Fraction
FAO	Food and Agricultural Organization
G	Soil Heat Flux
GDP	Gross Domestic Product
H	Sensible Heat Flux
IUCN	International Union for Conservation of Nature
LAI	Leaf Area Index
LAS	Large Aperture Scintillometer
LE	Latent Heat Flux
LULC	Land Use Land Cover
MAD	Mean Absolute Difference
MBE	Mean Bias Error
METRIC	Mapping Evapotranspiration at High Resolution With Internalized Calibration
MODIS	Moderate Resolution Imaging Spectroradiometer
MSL	Mean Sea Level
NASA	National Aeronautics and Space Administration
NCDC	National Climatic Data Centre
NDVI	Normalized Difference Vegetation Index
NOAA	National Oceanic and Atmospheric Administration

PMD	Pakistan Meteorological Department
RMSE	Root Mean Square Error
S.D.	Standard Deviation
SAVI	Soil Adjusted Vegetation Index
SEBAL	Surface Energy Balance Algorithm for Land
SEBS	Surface Energy Balance System
Sim-ReSET	Simple Remote Sensing EvapoTranspiration model
SSEB	Simplified Surface Energy Balance
T_s	Land Surface Temperature
USGS	United States Geological Survey

ABSTRACT

Evapotranspiration (ET) plays a major role in maintaining water balance and studying its spatial and temporal variations. It helps in irrigation planning and water resource management. It is very difficult to measure ET in field, and is estimated by indirect methods. Satellite remote sensing data in this respect is helpful for estimation of ET at large scales. In this study, the actual evapotranspiration was estimated using METRIC model employing Landsat 5 TM, Landsat 8 and meteorological data in Peshawar basin for time period 1998-2000 and 2009-2013. The land use land cover classification was carried out for the basin using ISODATA clustering. The model was validated against the reference ET calculated using FAO-56 Penman-Monteith equation and the estimates agreed well with R^2 = 0.70. The ET of tehsils were calculated by overlaying tehsils boundary and the ET of agricultural land use was also calculated. The results show that over the years, sugarcane and tobacco have increased, whereas, wheat-maize cropping decreased. The ET increased from March and was highest in summers and then decreased being lowest in winter. The ET over Charsadda, Mardan and Takht Bhai was highest (2 - 6 mm) and lowest in Peshawar (1.4 - 4.2 mm). The ET of sugarcane and tobacco was highest (1.7 – 5.2 mm) and lowest for wheat-fallow cropping system (0.4 – 3.3 mm). The ET of Kharif season in 2013 was highest near rivers, whereas in the Rabi season, ET was highest near Peshawar and Pabbi. The impact of variables on ET showed that combined R^2 was 0.68. These ET maps can help in irrigation planning, and monitoring crop water use over time and tehsil level ET maps can help in devising strategies to reduce water loss by water conservation efforts.

INTRODUCTION

1.1   Background

Water is a critical resource for every country necessary for maintaining food security and other economics of country. Water availability is a big player in the prosperity of countries as agricultural and industrial sector both require huge amount of water and compete for water resources. Hence, water scarcity poses a great challenge for nations especially developing countries due to climate change, increased water demand, environmental problems etc. The decreased flow of rivers and exploitation of groundwater above the limits further accelerates the problem of water scarcity for countries depending on river water for the agriculture which is the major user of fresh water globally.

Irrigated agriculture is a major consumer of fresh water consuming about 70% of world's freshwater available globally (Fischer et al., 2006). The rapid increase in the world population during early and mid-twentieth century and consequently increased food demand resulted in increase of irrigated area of world. World's 40% of irrigation is supported by flows from Himalayas and other large mountains. Irrigation is major source of food and provides the 40% of world's food from 20% of agricultural land. The increasing population put extra demand on food resources which is expected to rise to about 70% by 2050, doubling for developing countries. To match this food production, irrigated agriculture will require 11% increased water and of all the extra water demand of population growth in future, 40-100% will be required for agricultural production (Turral et al., 2011).

Agriculture consumes the 97% of freshwater in Pakistan forming an important part of hydrological cycle. 31.7 of 80 million ha (Mha) of area is under agriculture or forestry and 20.8 Mha is cultivated of which 80% is irrigated (Ullah et al., 2001). The increasing population and climate change has affected the canal irrigation and groundwater resources. Also there has been increasing competition for water resources between agriculture and industries. Hence, accurate estimation of water balance is necessary for understanding hydrological processes and irrigation planning. In many river basins, water demand exceeds availability. For example, in Indus basin, the available water is 274 billion m^3 of which 130 billion m^3 is available for use and 62 billion m^3 is lost excluding flow to sea. Also, the shortfall in water supply for agriculture purpose is about 20 billion m^3 (available 190 billion m^3 and demand 210 billion m^3) (Hussain et al., 2011). So, there is a need to assess water use to identify the direction of efforts of water management.

1.2   Evapotranspiration

Evapotranspiration (ET) is defined as the combination of two processes; evaporation of water from land and water surfaces, and transpiration of water from leaves of vegetation. In evaporation, vaporization occurs in which liquid water is converted to water vapour followed by the removal of water vapours from the surface which can be lake, river, ocean or any other water surface. Transpiration involves vaporization of water vapours from plant tissues into atmosphere. The two processes occur simultaneously and are difficult to separate. ET is normally estimated from the fraction of solar radiation reaching vegetation and the water available in top soil.

For the ET to occur, three factors are necessary that include supply of water, availability of energy for vaporization, and gradient in vapour pressure in atmosphere for ET continuation. The ET can be distinguished from the crop water requirement which are normally considered the same and are almost identical. Crop water requirement represents the water required by crops whereas, crop ET is the amount of water lost from crop. Crop water requirement is the water required to compensate for crop ET while irrigation water requirement is difference of water requirement and precipitation, and also include leaching and other water spent (Allen et a., 1998).

1.2.1 Units

Evapotranspiration is represented as water lost as depth measured in millimeters per unit time which can be hour, day, week, month or even growing period. The depth units can also be represented in per area units as one hectare equals 10,000 m^2 and mm equals 0.001 m. 1 mm water loss can be translated as loss of 10 m^3 of water per hectare. ET can also be represented in units of energy received per area as it is normally calculated as latent heat flux. This energy is heat of vaporization, the energy required for vaporization of water expressed as $MJkg^{-1}$ that depends upon temperature. The latent heat flux is expressed as $MJm^{-2}day^{-1}$ (Allen et al., 1998).

1.3   Types of Evapotranspiration

Evapotranspiration is basically divided into two types; reference evapotranspiration (ET_r) also said as potential evapotranspiration and actual evapotranspiration (ET_a).

1.3.1 Reference Evapotranspiration (ET_r)

Reference evapotranspiration is the case under ideal conditions where water is evaporated under unlimited moisture. It was originally defined as potential ET by Penman (1956) as transpiration of water in unit of time by well-developed, well watered, uniform height, short green crop shading the ground completely. ET_r is ET from some reference crop such as alfalfa or grass and used to standardize ET measurement. Grass is used as reference crop in humid and sub-humid areas whereas alfalfa is used in arid and semi-arid (Al-Kaisi, 2000). ET_r is only dependent upon climatic factors and is independent of crop type or soil moisture and is calculated from weather data.

1.3.2 Actual Evapotranspiration (ET_a)

The actual water used and transpired by crops, soil and vegetation in available energy and soil moisture conditions is better represented by actual evapotranspiration (ET_a) which is water transpired and evaporated from soil and vegetation in available energy and soil moisture conditions (Senay et al., 2007).

1.4 Factors affecting Evapotranspiration

There are many factors which affect the ET and can be grouped into broadly three categories; climatic parameters, crop parameters and environmental parameters. ET_r is only affected by the climatic parameters due to non-dependence on crop or soil factors, whereas, ET_a is affected by all these parameters and is thus complex and difficult to estimate.

1.4.1 Climatic Parameters

Climatic parameters control the energy and removal of moisture from atmosphere. The major climatic parameters affecting ET include solar radiation, air temperature, humidity and wind speed.

Solar radiation is the largest source of energy for ET. The more the amount of energy reaching earth's surface, higher the ET, also the position of sun and clarity of atmosphere affects ET. The increased solar radiation increases the air temperature which increases ET and hence, it is higher in sunny, warm days and less in cold and cloudy days.

When the air humidity is high, air is saturated, has more moisture and less capacity of holding extra moisture, so ET is less. In dry atmosphere, the air has less moisture and can hold more moisture, so ET is high. The difference in vapour pressure between surface and surrounding air affects the moisture removal capacity. If the difference is high, ET will be high and vice versa.

Wind speed is responsible for replacing the air above surface with air from surrounding areas which removes water vapour. When ET occurs, the air above gets saturated and it is replaced with adjacent air masses which facilitates ET. When wind speed is high, the air is replaced quickly that increases ET (Allen et al., 1998).

1.4.2 Crop Parameters

Various crop related parameters affect ET in complicated ways which include but are not limited to crop type, variety, development stage, height, roughness, reflection, ground cover. Further, the diseases and stressed crops have different ET (Brown, 2014).

1.4.3 Environmental Parameters

Various environmental parameters affect ET. The factors like soil salinity, soil fertility, fertilizer application, soil structure, diseases, and pesticidess can all affect and reduce ET. Other factors that affect ET include plant's density and soil water content. For example, increased soil water content can increase ET but excess of soil water may result in waterlogging hampering crop growth which can reduce ET (Brown, 2014).

1.5   Importance of Evapotranspiration

ET is the major part of energy and water balance necessary for maintaining heat exchanges between land and atmosphere (Mutiga et al., 2010). It is a link between energy and water cycle in the form of latent heat flux which; always involve ET and heat of vaporization, a significant source of heat in atmosphere (Vinukollu et al., 2011). In agricultural sector, it is important to identify water deficiency, crop stress, and crop water use (Hadjimitsis and Papadavid, 2013). It helps in studying the relation between climate and vegetation and its monitoring is necessary for maintaining agricultural production and tracking depletion of water resources (Maeda et al., 2011).

Monitoring spatial and temporal variability of ET is necessary for most of water related applications and maintaining irrigation in river basins (McCabe & Wood, 2006). It is also important for tracking evaporative depletion and studying its variability with respect to climate, soil moisture, crop factors etc. (Yang et al., 2012). ET in combination with land use information help in allocation of water to different sectors like agriculture, natural environment, industries etc. and help in

monetizing the water use (Bastiaanssen et al., 2005). It is important for studying climate change patterns and, land surface processes, and also an important input in many models for analysis of global climate, floods, drought and other processes (Fisher et al., 2008; Maeda et al., 2011).

1.6   Problem Statement

The most significant but limiting factor in crop growth and irrigation is water. Evapotranspiration losses in semi-arid or arid regions with less rainfall can account for most part of water budget. Pakistan is an agrarian country with agriculture contributing 21% of GDP (Pakistan Bureau of Statistics, GoP, 2010). Majority of area is irrigated by Indus River and others are rain fed and irrigated by groundwater. Since 70% (90% in arid) of precipitation is lost as ET, studying ET in these areas are necessary.

Measurement of ET is an arduous task under varying climate, vegetation and terrain. It has traditionally been carried out by multiplying the ET_r by crop coefficients (K_c) according to crop type and stage of growth (Mutiga et al., 2010). The potential evapotranspiration ET_o is not representative of actual water use by crops and differs significantly from actual evapotranspiration ET_a due to vegetation, soil texture, phenology, diseases, drought etc. (Anderson et al., 2012). In field, ET has historically been measured based on pan evaporation and lysimeters. In addition, methods like Bowen ratio system, sap flow meters and eddy covariance technique can be used for measuring ET at specific sites.

Most of these techniques are based on equations, assumptions and are indirect. Water balance studies rely on the accuracy of percolation measurement for ET estimation and Bowen ratio energy balance systems depend on sensor

accuracy for measurement of humidity. The eddy-covariance under-estimates energy and vapor fluxes whereas, lysimeter accuracy depend upon precision of installation and representation of real conditions (Bastiaanssen et al., 2005). Also, these techniques are expensive, complex, accuracy demanding and cannot be applied to very large areas or river basins (Rasul and Mahmood, 2009). ET is normally estimated rather than actual measurements which has led to the development of many indirect methods and models for its estimation.

Remote sensing is an indirect method that can help in ET estimation over large areas without the challenging task of setting field monitoring networks. Spatial coverage is not only available at basin scale but also at field and project scales. The data are also available at fixed temporal scale. The radiance measurements of the satellites can easily be converted into ET estimates. Parameters such as albedo, vegetation cover, surface temperature, Leaf Area Index (LAI), and radiation can be retrieved from the satellite image using visible, near-infrared and thermal infrared spectral bands (Li et al., 2012). In contrast to measurements only at a few points, satellite data provide measurements at continuous spatial scale and high spatial resolution. Landsat satellite data provides estimates at 30 m resolution which increases accuracy than Moderate Resolution Imaging Spectroradiometer (MODIS) at 1 km resolution. Spatial resolution of MODIS prevents the study of field scale variability. A pixel of Landsat can easily cover a typical field size of 0.1 ha (30 x 30 m) in developing countries, and at this resolution, variability in ET within a field can be studied easily and more accurately (Anderson et al., 2012).

The arid and semi-arid climatic conditions of Pakistan have major impact on ET. The changing climatic conditions of Pakistan due to global warming are evident from warm climate and the expected temperature changes in this region are higher than other parts of world. Also, its rivers are fed by Hindu Kush-Karakoram-Himalayan glaciers which are under serious threat of melting due to global warming (Hussain et al., 2005). Irrigation in river basins of Pakistan also use large amount of water that increases water losses from plants. Kabul River is also fed by mountains in northern Pakistan and Afghanistan which are also affected by climate change. Already the flow of Kabul River at Attock has decreased from 34.6 to 23.5 km^3 over the years and erratic monsoonal rainfall over 70 years resulted in decrease in seasonal flows (IUCN, 2010). All these factors have impact on water resources of country and hence, evapotranspiration. Therefore, monitoring and studying variability of ET in Peshawar basin can help in studying the effect of climatic changes on water resources and irrigation. It can also help in studying drought risk affecting the food security.

1.7   Objective

The objective of this study is to "Estimate the actual evapotranspiration using Mapping Evapotranspiration at high Resolution with Internalized Calibration (METRIC) model" using Landsat data. It will be further expanded to assess and analyse;

- The impact of land-use on evapotranspiration,
- The trends of climatic variables in relation to evapotranspiration, and
- Useful data in form of accurate estimates of ET for the hydrological models of the region.

1.8 Organisation of Study

This thesis is divided into five chapters. Chapter 1 describes the background of the study and introduces the basics, types, importance and factors affecting ET. It briefly explains the problem statement, objectives of study and thesis structure.

Chapter 2 reviews the literature of ET and describes the various methods of ET estimation. It describes the direct and indirect estimation methods including ET_r methods, field estimation and remote sensing. It describes in detail remote sensing based methods for ET estimation, the SEBAL and METRIC model and presents various researches employing these models. It then discusses the validation studies of these models and their comparison and relative accuracy with other models. The effect of spatial resolution on ET is also reviewed and the ET studies in Pakistan are also discussed.

Chapter 3 describes the study area and methodology of research. It includes overview of study area, data collection, data pre-processing, land use land cover classification, ET_r calculation, estimation of various biophysical parameters, and finally the detailed procedures of METRIC model.

Chapter 4 presents results of the study including classification, its accuracy, and change detection. It then describes the model validation, model results, the daily and seasonal ET variations, the ET of different crops, ET of tehsils and finally the impact of various climatic and biophysical variables on ET.

Chapter 5 presents the conclusion of study, limitations of work, future scope and final recommendations.

LITERATURE REVIEW

This chapter presents methods of ET estimation with remote sensing methods in detail with their validation and comparison studies. Also, the effect of spatial resolution on ET and different ET studies in Pakistan are discussed.

2.1 Evapotranspiration Estimation Methods

Various ET estimation methods have been developed over time. These methods measure ET based on various properties such as climatic parameters, vapour transfer measurement, water balance, atmospheric stability etc. Three broad categories of ET estimation methods are; (i) Direct field measurement methods, (ii) Indirect estimation methods and (iii) Remote sensing based methods.

2.1.1 Direct Field Measurements

The direct field measurement techniques are based upon either measurement of ET as a loss of water by measuring other components or the measurement of water vapour flow as mass or energy balance by different sensors (Shuttleworth, 2008). These methods measure ET mostly at field scale except water balance technique which is applicable at basin scale.

2.1.1.1 Water Balance

In water balance or also called soil water balance, ET is measured as a residual term in water balance where all other components of water balance are measured and the difference of these components results in ET. This method is based on the law of conservation of mass where the unmeasured difference in the water balance equation is the ET (Rana and Katerji, 2000). The incoming and

outgoing water from soil is measured where irrigation and rainfall add water to soil and soil water evaporation and crop transpiration remove water. The ET is measured from assessing change in soil water content but this method can only give ET estimates over week or longer (Allen et al., 1998) as it gives area-weighted measurements which can be difficult and expensive to measure for components like soil moisture and groundwater (Shuttleworth, 2000).

2.1.1.2   Lysimeters

The basic principle of working of lysimeter is water balance but the difference in this case is that the same conditions are matched in a container where the measurements are done. In a separate tank the soil is placed and plants are grown where the water movement is measured and water balance equation is solved with ease. In weighing lysimeters, water loss is measured by change in mass, whereas, in non-weighing lysimeters, water loss is estimated from the drainage water in tank after use. One major requirement for accurate estimation is to exactly match the conditions in tank to field conditions, otherwise it will result in erroneous results. The lysimeters are dependent upon sample and are often not representative of field and represent point measurements (Rana and Katerji, 2000). They are also expensive and difficult to operate (Allen et al., 1998).

2.1.1.3   Bowen Ratio

Bowen Ratio measures the ET by energy balance. Bowen ratio towers are used to measure ET in field by sensors that measures differences in air temperature, CO_2, moisture content between two heights that are used to calculate energy balance terms (Glenn et al., 2007). The major drawback is that it is

unsuitable for tall vegetation and measurement near dawn or dusk (Shuttleworth, 2008).

2.1.1.4 Eddy Covariance

Eddy covariance technique is based upon the vertical wind fluctuation in relation with vapour density (Glenn et al., 2007). It is basically based upon concept of eddies which are air parcels that move up or down in air due to difference in temperature and moisture. Instruments measure the wind fluctuations along with temperature and moisture which are used to calculate energy balance terms from which ET is calculated as 20-60 minutes average (Shuttleworth, 2008).

2.1.1.5 Large Aperture Scintillometer (LAS)

LAS uses a light beam to measure the vertical wind fluctuations caused by eddies formed due to temperature and air moisture difference from which sensible and latent heat can be measured. Due to the effects of wind, sensible heat is estimated over an area rather than point measurement from light beam which can extend up to several kilometres. This method has bigger scale than other direct field measurement methods and applied from field to landscape scale (Kite and Droogers, 2000; Shuttleworth, 2008).

2.1.2 Indirect Estimation Methods

As the field methods of ET measurement are expensive and difficult to operate, ET is computed mostly from the weather data obtained from weather stations including temperature, humidity, wind speed, and vapour pressure etc. These weather data are used to compute ET_r from which ET of crop is calculated using crop coefficients (K_c). The ET_r estimation methods fall into three categories i.e. combination, radiation and temperature methods.

2.1.2.1   Combination Methods

The combination methods utilize both radiation and temperature measurements in the calculation of ET_r. These methods require the extensive amount of good weather data. Combination methods include Penman Method and FAO-56 Penman-Monteith method. Penman method was given by Penman (1948) and uses the weather data of radiation, pressure, temperature and wind speed. It was developed to remove the need of surface temperature and to measure evaporation from open water but is used for well watered crops (Dodds et al., 2005). It uses aerodynamic approach i.e. the difference of temperature between two heights along with net radiation not considering any ground heat exchange or storage.

FAO-56 Penman-Monteith method is standard method for calculating ET_r (Allen et al., 1998) and uses aerodynamic components and surface resistance for calculating ET_r which requires large amount of data. This method uses the reference crop at height of 0.12 m with surface resistance of 70 sm^{-1} and albedo 0.23 for calculations. These conditions are typical of uniform, healthy and well-watered green grass. Using a reference crop for calculations allows the method to serve as standard for comparing ET at different times, places and crops.

2.1.2.2   Radiation Methods

Radiation methods remove the need of humidity and temperature data and most common is Priestley-Taylor method (Priestley and Taylor, 1972). This method does not use wind speed and humidity data and calculates ET_r without aerodynamic component. It measures ET from well watered evaporating crops by

using an empirical coefficient of 1.26. It is not suitable for measurement in arid irrigated crops (Dodds et al., 2005).

2.1.2.3   Temperature Methods

Temperature methods use temperature data in ET estimation. These methods are used when other data are not available. Hargraeves and Blaney-Criddle are two common methods of ET estimation. Hargraeves method uses a relationship between temperature and humidity, whereas, Blaney-Criddle uses mean temperature and sunshine hours for ET calculation.

2.1.2.4   Crop ET from Crop Coefficient

The crop ET is found out using crop coefficients which are developed according to crop growth and parameters. The crop ET_r is related to crop coefficient K_c in $ET_r \times K_c$ form to find out actual crop ET. K_c represents the crop canopy and resistance and represents specific crop characteristics. K_c is affected by crop type, climate, soil evaporation and crop growth stages (Allen et al., 1998). This method is the main method for irrigation scheduling and FAO maintains databases of K_c (Glenn et al., 2007).

2.1.2.5   Crop ET from Pan Evaporation

The evaporation from pan represents the effects of various factors on evaporation of water including temperature, humidity and wind. Generally, when there is no precipitation, evaporation from pan is measured as decrease in depth of water in mm. But the water lost by evaporation is significantly different from the water lost from crops and is higher than crop ET. The radiation from pan can be different, the heat storage in pan can also cause evaporation at night and also the temperature, humidity conditions above pan can all result in different ET. So pan

evaporation is related to ET_r using pan coefficient K_p by the function $ET_r = K_p \times Pan$ evaporation (Allen et al., 1998).

2.1.3   Remote Sensing Methods

Remote Sensing methods have been developed recently and put into use the various kinds of satellite data including National Oceanic and Atmospheric Administration's Advanced Very High Resolution Radiometer (NOAA/AVHRR), MODIS and Landsat. The satellite data provides the measurements for large areas and help in effective study of spatial variations. They have advantage over other methods due to their less cost and ease of applications. Remote Sensing methods for ET estimations are diverse. Two broad categories of methods based on remote sensing are using vegetation indices and using surface energy balance approaches.

2.1.3.1   Vegetation Index Methods

These methods make use of various vegetation indices developed from the satellite data for calculation of ET as these indices are representative of vegetation density and amount. NDVI is most common vegetation index with SAVI being another one. LAI is another index that commonly used for ET estimation that represents ratio of leaf area to ground coverage. Another measure is fractional cover (f_c) which is fraction of ground covered with vegetation. Usually these indices are used in place of K_c for estimation of ET (Glenn et al., 2007). One drawback of this method is requirement of ground calibration.

Nagler et al. (2005) estimated ET using MODIS and in situ measurements of ET from bowen ratio and eddy covariance towers from riparian vegetation along western US rivers. Enhanced Vegetation Index was calculated from MODIS which was strongly correlated to ET estimates from towers and with inclusion of air

temperature the correlation improved further. 16 day composite of vegetation index and temperature were used to predict ET (R^2= 0.74) and regression equation was developed to scale ET values over four years. The study found out lower estimates of ET than those from water budget estimates of area. In another study, Nagler et al. (2013) estimated ET of riparian and agricultural vegetation using ET_r and MODIS enhanced vegetation index and the algorithm was calibrated with ET from eddy covariance towers with R^2 of 0.73. The results were compared with water balance and tower data and errors were within 10%. The study concluded that the model could be used for estimating ET using vegetation and ET_r data over dry land irrigated and riparian areas but cannot be extended to other areas.

2.1.3.2   Surface Energy Balance Methods

Surface energy balance methods make use of the satellite data for estimating various components of energy balance i.e. net radiation, soil heat flux and sensible heat flux and calculate ET as a residual of these components. They involve conversion of satellite data into variables like albedo, reflectances, vegetation indices, surface temperatures that are used to calculate energy balance and aerodynamic functions.

Senay et al. (2007) used Simplified Surface Energy Balance (SSEB) model with MODIS NDVI and thermal data to measure seasonal ET in irrigate agriculture river basin Kabul and Helmand in Afghanistan over six years (2000-2005). They found that cropping patterns of region affected temporal ET representing water use pattern. Bawazir et al. (2009) calculated ET using surface energy balance approach with National Aeronautics and Space Administration (NASA) Terra Advanced Spaceborne Thermal Emission and Reflection Radiometer (ASTER) satellite data

in RioGrande Basin, USA and compared the estimates with eddy covariance flux towers. They found out the Mean Square Error (MSE) for saltcedar and cottonwood as 0.16 and 0.37 mmday-1 and the variations in ET were due to plant type, density, soil type, moisture and water table depth.

Sun et al. (2009) developed a dual.-source Simple Remote Sensing EvapoTranspiration model (Sim-ReSET) based on only RS data. In this model aerodynamic resistance calculation was avoided by reference dry bare soil and homogenous wind speed assumption. The test with ground observations resulted in root mean square error (RMSE) of 41.84 Wm^{-2} and mean absolute difference (MAD) of 34.27 Wm^{-2} under neutral atmospheric conditions and RMSE of daily ET for cloudless days was 0.30 mm day^{-1}, and the MAD was 0.26 mm day^{-1}.

Jin (2009) computed ET using Surface Energy Balance System (SEBS) with cloud free AVHRR images over period from 1990-2004 in Zhangye basin, China. He found out that the annual ET increased gradually over years at rate of 0.21×10^8 m^3 per year due to increase in vegetation cover. Li et al., (2012) used data from AVHRR with meteorological and in situ data to estimate ET over Heihe River Basin with evaporative fraction model and found out higher ET values in inland river basin than in heterogeneous areas and desert where vegetation is dense and continuous and vary with crop development stage. They also found that high soil moisture can result in high ET despite of low vegetation and cloud cover can also give high ET.

2.1.3.3   Other Empirical Methods

Apart from vegetation index and energy balance models, there are also some other models of estimating ET using remote sensing. Some of them attempt

to make use of standard ET_r algorithms by incorporating the parameters computed from satellite data. Farg et al. (2012) used SPOT-4 satellite data to compute K_c for wheat crop and integrated it with ET_r computed from FAO Penman-Monteith method. NDVI and SAVI were calculated from SPOT-4 images from which K_c prediction equations were developed by multiple regression for developing, mid-season and late-season. Some of them are based on hydrological modelling approaches employing various hydrological models to compute ET. Some of the global ET products have also been made available by satellites data distributors. For example, MODIS have 8-day ET product MOD16 (Mu et al., 2011).

2.2   Surface Energy Balance Algorithm for Land (SEBAL)

Among the various remote sensing based models, more common and with fewer requirements of ground data is SEBAL which has become one of the most successful models. It was first derived by Bastiaanssen in 1998 (Bastiaanssen et al., 1998) for Egypt, Spain and Niger and then applied for more than 30 countries (Bastiaanssen et al., 2005). Various studies have used SEBAL for ET estimations. Ahmad et al. (2005) used SEBAL to assess ET in Olifants Basin, South Africa using Landsat 7 ETM+ data of rainy season and found that the ET was highest for irrigated areas and higher than ETr value from Penman-Monteith equation. 25% of ET was from agricultural land use and irrigation contributed about 4% of basin ET.

Ahmad et al. (2006) computed ET in Krishna Basin, India using Landsat 7 image with SEBAL and found out that irrigated agriculture ET depends upon the crop growth stage. They found out that wastewater irrigated area had highest ET and grass ET was lowest. Teixeira et al. (2009) used Landsat from 2001 to 2007 and agro-meteorological data with SEBAL to compute ET, biomass and crop water

productivity in Low-Middle Sao Francisco River Basin, Brazil. They found out that ET for irrigated crops was higher than vegetation.

Mutiga et al. (2010) used SEBAL with MODIS to estimate spatio-temporal patterns of ET_a in drainage basin upper Ewaso Ng'iro North, Kenya for 2000, 2003 and 2006. They found that ET increased gradually with rate of 15% and that NDVI and altitude have high impact on ET with R^2 of 0.6048 and 0.32 respectively. They compared results with water balance and obtained correlation of 70%. They also found that although SEBAL overestimated ET as compared to FAO-56 method estimated, the estimates correlated well with one another with R^2 0.7499.

Sun et al. (2011) estimated ET in Nansi Lake Wetland of China using SEBAL with Landsat 7 ETM+ images, DEM and Meteorological data. They compared the ET estimates from SEBAL with those obtained from pan observation data and found overestimation with 10.8% of deviation from daily estimates which was considered reasonable. Yang et al. (2012) estimated ET using SEBAL with MODIS data in an irrigation district of North China from 2000 to 2010. They found that ET over agricultural areas is controlled by Reference ET which is affected by crops whereas in other areas, precipitation affects ET. They tested the SEBAL performance against in situ measurements on field scale, and water balance modelling at regional scale. They found relative error of 14.6% at field scale on 5–7 days basis and 5.6% at regional scale on annual basis.

Li et al. (2013) used SEBAL with Landsat 5 data to compute ET of Yellow River source region in 2006 and found that ET was highest in grassland and lowest in bare soil. They also computed the relation of biophysical variables with ET and found out that temperature has highest correlation of -0.802 with ET. Du et al.

2013 used SEBAL with MODIS and meteorological data to compute ET over Sanjiang Plain, China for 2006 growing season. They found out that SEBAL misestimated at 10.52% compared to eddy covariance and was within 8.86% deviation from ground observation. They found out that ET increased up to June or July and then decreases with vegetation.

SEBAL has been validated and found that the seasonal ET were within 5% error of other ET methods and daily ET were less than 15% (Bastiaanssen, 2010). Thoreson et al. (2009) compared ET estimations from SEBAL (based on Landsat), water balance and crop coefficients approach and found that SEBAL estimations were close to water balance with less than 1% difference as compared to difference of 14% for crop coefficient approach. The monthly percent difference varied from -2.7% to just over 30% due to error in soil water storage calculation, whereas, annual estimate have less error.

2.3 Mapping Evapotranspiration at High Resolution with Internalized Calibration (METRIC) Model

The original SEBAL has been modified to improve estimations and developed into METRIC model (Allen et al., 2007). There are two main modifications i.e. METRIC model includes topographic corrections in various parameters including surface temperature, roughness and wind speed by adding elevation information from Digital Elevation Model (DEM). Inclusion of elevation information helps in getting realistic estimates of ET over mountainous areas by correcting surface temperature which would otherwise lead to ET over estimation. Secondly it uses ET_r in the calibration of model instead of net radiation. This provides the equivalency of ET with ET estimated using crop coefficient approach

and removes biases in energy balance terms. The internal calibration can reduce bias in ET by 30% as compared to other methods (Allen, 2006).

Gowda et al. (2008) used METRIC model with Landsat TM to compute hourly ET of Texas High Plains. They compared computed fluxes with those from lysimeters and found good agreements for irrigated and dry land field. Dry land experienced some high errors due to hot pixel selection errors. Chávez et al. (2011) applied METRIC model on high resolution aircraft images (0.5-2.0 m pixel) acquired over semi-arid Southern High Plains during 2007 summer cropping season. The daily ET estimates were compared to lysimeters and errors were 2.4 $\pm$ 9.3% and hourly ET errors were 0.7 $\pm$ 11.6%.

One of the important considerations in METRIC is extrapolation of instantaneous estimates in daily and seasonal estimates. For daily estimates METRIC assumes constant evaporative fraction and for longer periods monthly or seasonal evaporative fraction is taken constant for period, linearly interpolated or a cubic spline interpolation is done. Singh et al. 2012 studied these three methods for extrapolation from METRIC ET in growing season in mid-west USA. They found model estimated ET compared well to eddy covariance with R^2 of 0.91 with standard error of 20%. They also found that there was no statistically significant difference between cubic spline, fixed and linear interpolation.

The estimates of METIC are affected by various variables including albedo, temperature, cold and hot pixel selection etc. Choragudi (2011) carried out sensitivity analysis of various METRIC parameters using Landsat to determine the highest influencing parameter. He divided the errors in two kinds; global errors like reflectance, transmittance, temperature, wind speed, ET_r which are

compensated by calibration and local errors like pixels selection, roughness, soil heat flux which are not compensated in calibration. He found that METRIC can compensate most global errors but the parameter most sensitive is selection of hot and cold pixels. Roughness was insensitive, the temperature difference function was more sensitive for bare soils and other local errors were linearly proportional to errors. In another sensitivity analysis of METRIC using Landsat by Mokhtari et al. (2013), temperature difference at two heights, surface temperature, net radiation, sensible heat flux, surface albedo, soil heat flux, and air temperature were found to be highly sensitive variables.

METRIC has also been validated by various studies. In one of the study by Mkhwanazi and Chávez (2012), METRIC was used to compute ET using Landsat 5 TM and Landsat 7 ETM for growing season. The ET was compared with lysimeters and other ground measurements and the RMSE was found out as 0.14 mmh^{-1} (17.6%), Mean Bias Error (MBE) of -0.08 mmh^{-1} (-10.3%) and an R^2 of 0.83.

The relative accuracy of METRIC and SEBAL has also been studied in comparison with ground measurements. Mkhwanazi et al. (2012) compared the SEBAL and METRIC ET estimates with Large Aperture Scintillometer estimates and found METRIC accurate than SEBAL. They found that for hourly ET, the relative error of SEBAL was up to 38% while METRIC error was 11%. On comparison with weighing lysimeters, Mkhwanazi and Chávez (2012) found that SEBAL error was 45% whereas, METRIC error was 25%. They also found out that windy and hot days caused larger errors.

2.4 Effect of Spatial Resolution on Evapotranspiration

Spatial resolution also affects the derived estimates of ET. Currently AVHRR, MODIS, ASTER and Landsat with spatial resolutions of thermal bands as 1 km, 1 km, 90 m and 120/60/100 m respectively are used for ET retrieval. Low resolution satellites are effective for regional and global scale estimations but are unable to meet the requirements of spatial details for field scale research, water budget and ET estimations. Although the satellites like MODIS have high temporal coverage of 1 day, their coarse resolution inhibits their usage for practical and operational uses. The resolution of Landsat is effective for studying crops at field size (Anderson et al., 2012).

Kustas (2004) used Landsat to vary its resolutions from 60 m to 120, 240 and 960 m and computed the ET which was compared with tower and air-craft based measurements. They found out that at resolutions near 1000 m variation in field-scale ET was not feasible. They also noted that thermal sharpening for surface temperature can help distinguishing field-scale ET. At 240 m also, the ET is difficult to distinguish. The study concluded that only resolution less than 500 m can distinguish between land types. McCabe & Wood (2006) compared thermal bands of three sensors Landsat-ETM, ASTER and MODIS against eddy covariance measurements. They showed that higher resolutions like Landsat and ASTER are appropriate for small watersheds due to their field scale estimations and agreed more with ground measurements. They also found that although MODIS estimate agree with regional averages, it is unable to discriminate field scale ET.

Ershadi et al. (2013) did a study to find out the effect of spatial resolution on ET estimates by aggregating Landsat 5 data to coarser resolutions. They

aggregated the data from 120 to 960 m and calculated land surface temperature for every resolution and the respective ET using SEBS. They found that the aggregation didn't affect land surface temperature but reduce ET estimations up to 15% at image scale and 50% up to pixel scale. The reason behind decrease in ET was reduction in aerodynamic resistance that depend upon land cover. Trezza et al. (2013) computed ET using METRIC by MODIS and Landsat data and employed cross-calibration technique using Landsat for MODIS. They found out that although MODIS produced comparable ET estimates by cross-calibration, the spatial distinguishing power is less.

2.5   Evapotranspiration Estimation in Pakistan

ET has traditionally been measured using water balance and meteorological data from weather station. Rasul and Mahmood (2009) computed evapotranspiration in various climatic conditions of Pakistan using radiation method, Modified Penman method, Bradley and Criddle Formula, FAO Penman-Monteith Equation. They found that FAO Penman-Monteith equation worked best in all climatic conditions.

Ullah et al. (2001) calculated the ET_r using FAO-56 Penman-Monteith method for the meteorological stations covering Indus River Basin from which the ET of 11 canal command areas of basin was found out by contour analysis. They found that annual ET_r was lower (1200-1300 mm) in upper and northeastern part of basin due to mild climate and higher (1700-2100 mm) in lower part covering Southern Punjab and Sindh. They found that ET is maximum in June and minimum in December. The Rabi crops had ETr in range 240-462 mm, whereas, Kharif crops ETr have large variations from 341-1004 mm and the spatial

variations in crops range from 14-50%. The study also found out that water demand of lower Indus is 50% higher than upper Indus and that the cropping patterns and intensities affect crop water requirement.

Only recently potential of remote sensing to estimate ET over large areas such as Indus River Basin has been realized. Sarwar and Bill (2007) used ASTER data for ET estimation in Indus Basin by surface energy balance approach and meteorological data. The ET estimated varied from 0-4.5 mmday^{-1} and were in close agreement with estimations from hydrological model CROPWAT. They found out that water evaporation was less than that from pan evaporation. The ET of sugarcane was less due to early growth stage and was higher for maize and cotton due maturity of crops.

Bastiaanssen et al. (2002) estimated ET using SEBAL in Pakistan. They used SEBAL with NOAA AVHRR, sunshine duration and wind speed data to estimate ET in irrigated Indus River basin and validated results using different field based models. Their accuracy varied from 0-10% on field scale to 5% at regional scale. They found that Rabi ET ranged from 300-400 mm and was higher for Punjab than Sindh. Kharif ET is higher (600 mm) than Rabi ET due to stronger radiations, precipitation and rice and sugarcane cultivation.

Sultan and Ahmad (2008) used SEBAL with Landsat 7 ETM+ and meteorological data for ET estimation in Chenab sub-basin of Indus Basin. The study found out that high ET is in upper areas of basin including Sargodha and Mandi Baha-ud-din and lowest in lower parts like Jhang. They compared the ET with the ET computed using K_c and ET_r and found that ET estimation accuracy was up to 95% in Faisalabad, 90% in Jhang and 83% in Sargodha.

MATERIALS AND METHODS

3.1   Study Area

Peshawar basin is an intermountain basin located between longitude 71.15^o and 72.45^o and latitude 33.45^o and 34.30^o with area approximately 5600 km^2 in Khyber Pakhtunkhwa. The major cities of basin include Mardan, Charsadda, Peshawar and Nowshera with Kabul River flowing from west to east into Indus River (Figure 3.1). It is present at southern foothills of Himalayas surrounded by mountain ranges of Khyber in northwest, Swat in northeast and Attock-Charat in the south. In southwest the basin is bounded by Indus River. It is a flat basin with average elevation of the basin around 300 m above mean sea level (MSL) which increases to above 500 m near mountains. The soils of basin consist of piedmont plain in the southwest, floodplain between Kabul and Swat rivers, Loess plain in central part of plain west of Charsadda and north of Kabul river. The basin is characterized by climate suitable for irrigation and various crops are grown (Nasreen 2006).
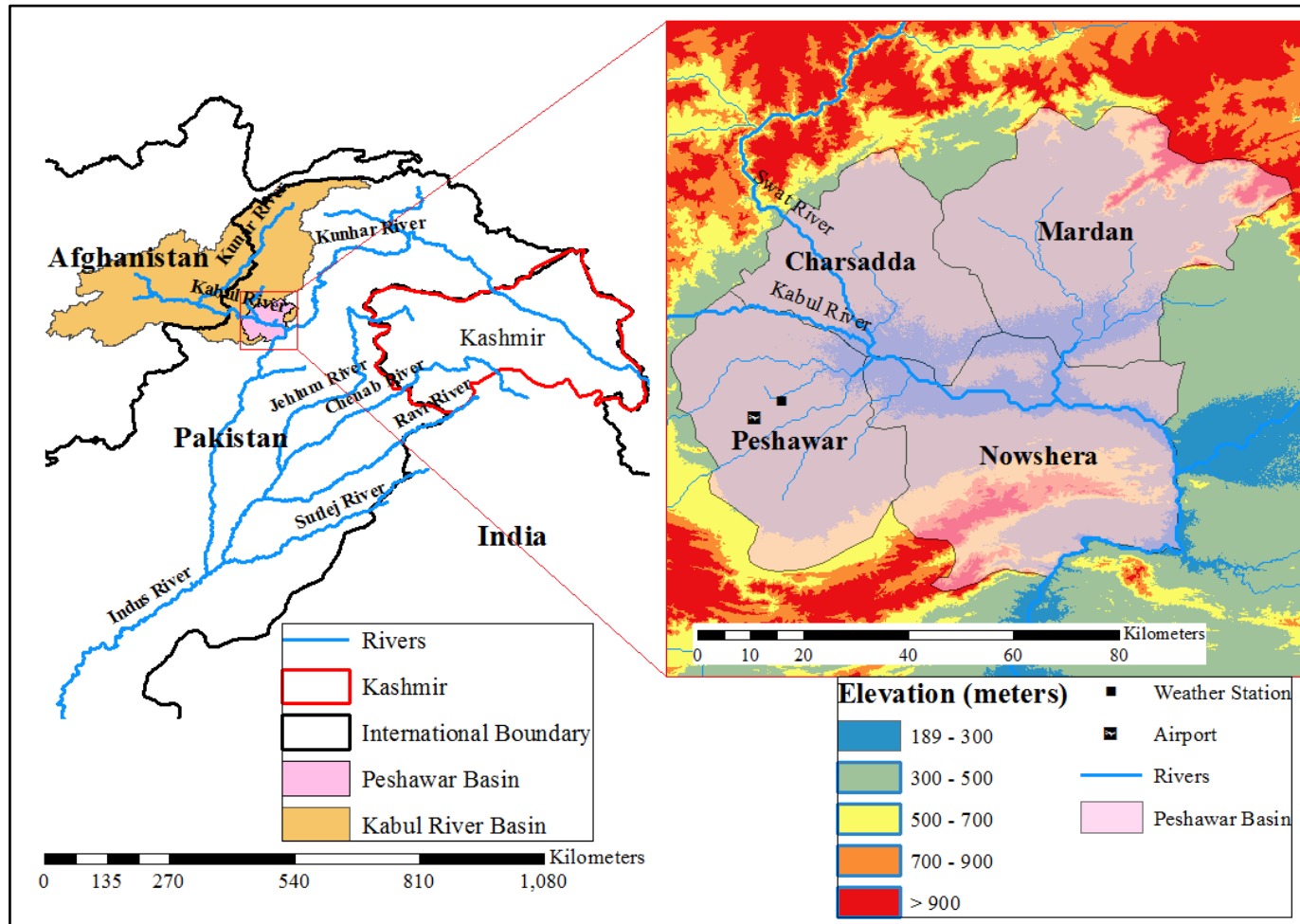
Figure 3.1: Peshawar Basin and its elevation

3.1.1 Climate

The climate of the basin is semi-arid in western part and sub-humid in eastern part with rainfall ranging from 300 mm to 630 mm per year. The hottest months are June and July with average daily temperature of 35-45°C; whereas, coldest month is January with average daily minimum temperature of 2-4°C (PMD NCDC, 2014). The mean annual potential evapotranspiration is approximately 1200 mm in Mardan and Nowshera, 1100 mm in Charsadda and 1500 mm in Peshawar. Figure 3.2 shows the mean monthly maximum and minimum temperatures, and cumulative monthly rainfall for the study area based upon meteorological data of Peshawar weather station.

3.1.2 Water Resources

Peshawar basin consists of four important rivers and nullahs namely, Kabul River, Swat River, Bara River and Kalpani nullah along with other perennial and non-perennial nullahs. Kabul River is the major river of basin dividing the basin into southern and northern parts. It enters the basin near Warsak, Peshawar from west and falls into Indus River near Attock. It is the major contributor to the flow to Indus River from Afghanistan with total inflow of 21.5 km^3 (15.5 km^3 from Kabul River and 6 km^3 from other tributaries) (FAO, 2011).

Swat River enter plain in northwest and discharge in river Kabul near Charsadda. Bara River enter the basin near Jhansi post from south which is diverted to canals for drinking and irrigation purposes. Kalpani Nullah arises in basin itself draining large area in north and discharges in Kabul River. Apart from surface water, groundwater is also used as water source for drinking and irrigation purpose with 609 tube wells for domestic water supply in villages and cities.
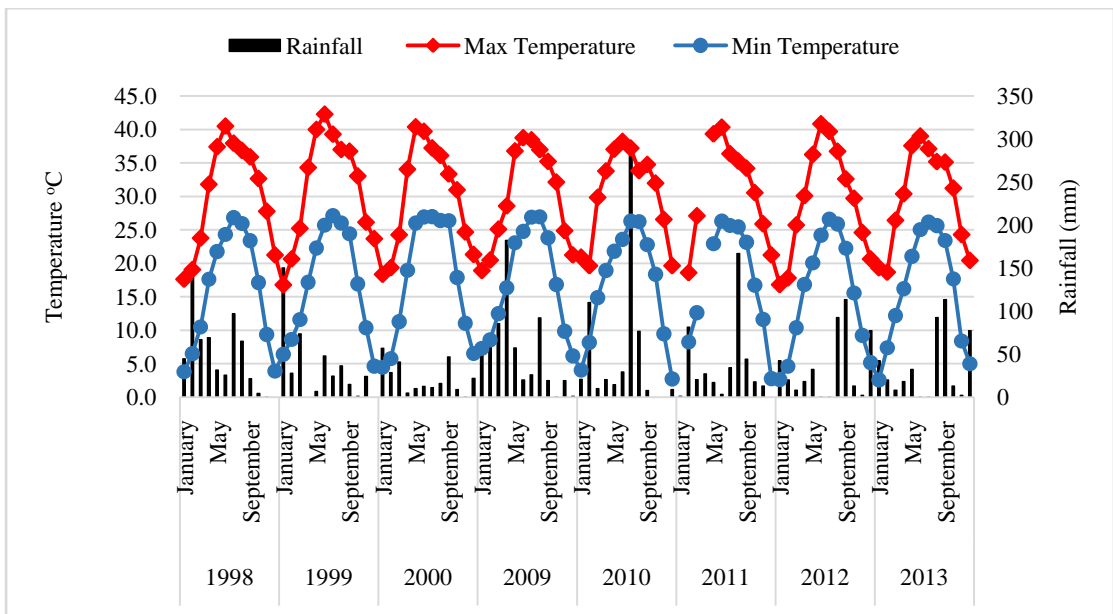
Figure 3.2: Mean monthly maximum and minimum temperature, and cumulative monthly rainfall from 1998-2013

(Source: PMD)

3.1.3 Agriculture

The total cultivated area of the basin is 400,000 ha of which 65% is irrigated area (Khyber Pakhtunkhwa Development Statistics, 2010). The major Rabi crop involve wheat, tobacco whereas, Kharif crop include maize. The annual crops include sugarcane and fodder in addition to orchards. The crop calendar of the crops is given in figure 3.3.

3.1.4 Irrigation

Irrigation is carried out both by means of surface water and ground water. Surface water irrigation is dependent upon rivers and canals. The lower Swat canal starts from left bank of Swat River in northwest with commanded area of 52,000 ha between Charsadda and Mardan. The upper Swat canal drains from left bank of Swat River in Swat with command area of 112,000 ha. The Warsak high level left bank canal starts from Kabul River left bank upstream Warsak dam with command area between Kabul and Swat rivers. Kabul river canal takes off from right bank of Kabul river near warsak and Warsak high level right bank canal starts from Kabul River left bank upstream Warsak between left canal and Kabul River canal. In northeast of basin, Pehur canal starts from right bank of Indus River with command area 17,870 ha on both sides of canal. The largest canal is Jue Sheikh and private canals are situated in south and west of basin.

Dug wells and tube wells are used for irrigation with ground water with 190 tube wells irrigating 21,200 ha of area. Dug wells are used mostly in Charsadda and Mardan areas where water is raised by Persian wheels or under water pumps (Nasreen, 2006).

Crops	Jan	Feb	Mar	Apr	May	June	July	Aug	Sep	Oct	Nov	Dec
Wheat												
Maize												
Tobacco												
Sugarcane												
Fodder												

Cultivation

Harvesting

Cultivation and Harvesting
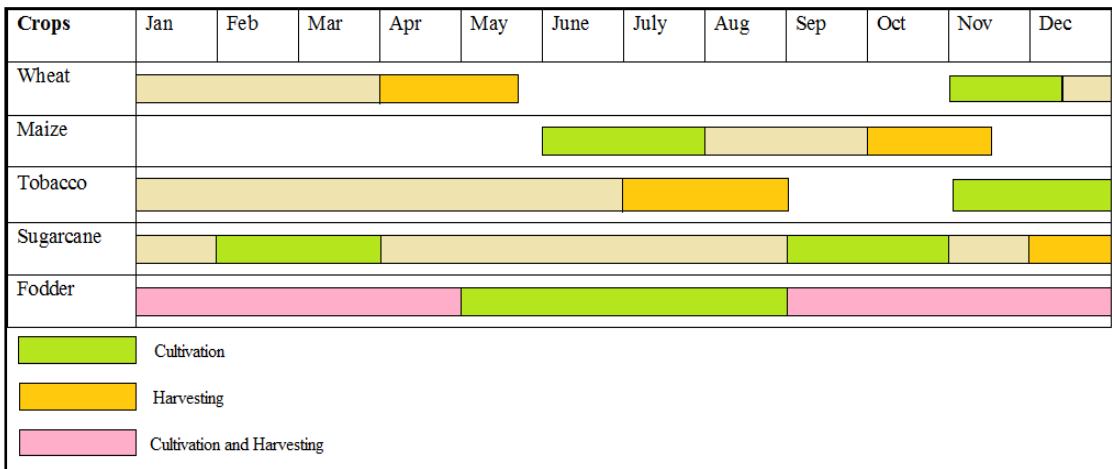
Figure 3.3: Crop Calendar of major crops in Peshawar Basin

3.2   Data Used

3.2.1   Remote Sensing Data

3.2.1.1   Landsat

Landsat satellite remote sensing program started in 1972 with its 1st satellite Landsat 1 and Landsat 8 being the latest satellite. The high spatial resolution and presence of thermal band makes Landsat suitable for evapotranspiration estimation up to field scale with good accuracy. The Landsat TM data for time periods of 1998-2000 and 2009-2011 and Landsat 8 data for year 2013 were acquired from USGS Earth Explorer website (www.earthexplorer.usgs.gov). The images with cloud cover less than 10% were selected according to the requirement of METRIC of cloud free images. The remaining cloud cover was removed as detailed in section 2.3.2. A total of 44 images were acquired for the Peshawar basin.

3.2.1.2   Digital Elevation Model (DEM)

METRIC requires topographic correction for reflectance and land surface temperature which requires a DEM. The 30 m ASTER DEM was acquired for the study area from USGS Earth Explorer website (www.earthexplorer.usgs.gov).

3.2.2   Meteorological Data

In addition to satellite data, METRIC model requires some meteorological data as input. The meteorological data with 24 hour time period for the study period was obtained from the Pakistan Meteorological Department's weather stations Peshawar and Balakot. Meteorological data of the study area include minimum and maximum air temperature, relative humidity, precipitation, sunshine hours and wind speed. The details are given in table 3.1.

Table 3.1: Meteorological data for METRIC

Parameter	Purpose
Wind Speed (km/hr)	Estimation of evapotranspiration
Precipitation (mm)	For evaluating wetness of image for calibration
Relative Humidity (%)	Calculation of reference evapotranspiration
Sunshine hours (hr)	Same as above
Min. Temperature (^{o}C)	Same as above
Max. Temperature (^{o}C)	Same as above

3.3   Pre-Processing

3.3.1   Image Calibration

The images were calibrated into radiance and reflectance.

3.3.1.1   Radiance

Radiance is the outgoing radiation observed at top of atmosphere by the satellite measured in $W/m^2/sr/\mu m$. It is calculated as follows for Landsat TM;

$$L_\lambda = \frac{L_{max} - L_{min}}{Qcal_{max} - Qcal_{min}} \times (DN - Qcal_{min}) + L_{min} \tag{3.1}$$

where;

- DN is the digital number of each pixel,

- L_{max} and L_{min} are calibration constants, and

- $Qcal_{max}$ and $Qcal_{min}$ are the highest and lowest range of values for rescaled radiance in DN.

For Landsat 8, radiance is calculated as;

$$L_\lambda = (M_L \times DN) + A_L \tag{3.2}$$

where;

- M_L = Band-specific multiplicative rescaling factor from the metadata

- A_L = Band-specific additive rescaling factor from the metadata

3.3.1.2   Reflectance

Reflectance is the ratio of reflected to incident radiation. It is calculated as follows for Landsat TM;

$$\rho_\lambda = \frac{\pi * L_\lambda}{ESUN_\lambda * cos\Theta * d_r} \tag{3.3}$$

where;

- L_λ is the spectral radiance for each band,

35

- ESUN$_\lambda$ is the mean solar exo-atmospheric irradiance for each band (W/m^2/µm)

- cosθ is the cosine of the solar incidence angle (from nadir), and

- d$_r$ is the inverse squared relative earth-sun distance.

For Landsat 8, reflectance is calculated as;

$$\rho_\lambda = \frac{M_\rho \times DN + A_\rho}{cos\theta} \qquad (3.4)$$

where;

- DN is the digital number of each pixel,

- M$_\rho$= Band-specific multiplicative rescaling factor from the metadata

- A$_\rho$= Band-specific additive rescaling factor from the metadata

3.3.2 Cloud Masking

All images were visually analysed for cloud cover and since the amount of cloud cover was less, a few remaining clouds were visually detected and masked using temperature and albedo thresholds.

3.4 Reference Evapotranspiration (ET$_r$)

As stated earlier, reference evapotranspiration is ET from some reference crop grass or alfalfa. The ET$_r$ in the present study was calculated using REF-ET calculator developed by Allen (2013) through FAO-56 Penman-Monteith equation which is standard method for calculating ET$_r$. It is calculated as;

$$ET_r = \frac{0.408\Delta(R_n\text{-}G) + \gamma\frac{900}{T+273}u_2(e_s\text{-}e_a)}{\Delta + \gamma(1+0.34\ u_2)} \qquad (3.5)$$

where;

- ET$_r$ is reference evapotranspiration [mm day^{-1}],

- R_n net radiation at the crop surface [MJ m^{-2} day^{-1}],

- G soil heat flux density [MJ m^{-2} day^{-1}],

- T mean daily air temperature at 2 m height [°C],

- u_2 wind speed at 2 m height [m s^{-1}],

- e_s saturation vapour pressure [kPa],

- e_a actual vapour pressure [kPa],

- e_s-e_a saturation vapour pressure deficit [kPa],

- Δ slope vapour pressure curve [kPa °C^{-1}],

- γ psychrometric constant [kPa °C^{-1}]

3.5   Biophysical Parameters

METRIC requires various biophysical parameters to be calculated from image including vegetation indices, surface albedo, surface emissivity, land surface temperature. These parameters were calculated as follows;

3.5.1   Vegetation Indices

Vegetation indices help to enhance vegetation. There are various vegetation indices of which Normalized Difference Vegetation Index (NDVI) is the most common. In this study, three kind of vegetation indices were calculated namely, NDVI, SAVI (Soil Adjusted Vegetation Index) and LAI. NDVI was calculated as follows;

$$\text{NDVI} = (\rho_4 - \rho_3) / (\rho_4 + \rho_3) \tag{3.6}$$

where;

- ρ_4 and ρ_3 are reflectivities for bands 4 and 3

SAVI was calculated as;

$$\text{SAVI} = (1 + L)\,(\rho_4 - \rho_3) / (L + \rho_4 + \rho_3) \tag{3.7}$$

where;

- L is a constant for SAVI taken as 0.5

LAI was calculated using equation from Bastiaanssen (1998b) as;

$$\text{LAI} = -\frac{\ln\{(0.69\text{-SAVI})/0.59\}}{0.91} \qquad (3.8)$$

3.5.2 Surface Albedo

Surface albedo (α) is the ratio of the reflected to incident shortwave radiation. It was calculated following Tasumi et al. (2008) as;

$$\alpha = \sum_{b=1}^{n} \rho_{s,b} \, w_b \qquad (3.9)$$

where;

- $\rho_{s,b}$ is the at surface reflectance
- ω_b is a weighting coefficient for each band.

3.5.3 Surface Emissivity

Surface emissivity (ε) is defined as the ratio of surface radiated thermal energy to the energy radiated by blackbody at same temperature. In METRIC two types of surface emissivities are calculated following Tasumi (2003);

- ε_{NB} representing thermal emission in band 6 (10.4 to 12.5μm)
- ε_o representing thermal emission in thermal spectrum 6 to 14μm

The emissivity was calculated as;

$$\varepsilon_{NB} = 0.97 + 0.0033 \, \text{LAI; for LAI} < 3 \qquad (3.10)$$

$$\varepsilon_o = 0.95 + 0.01 \, \text{LAI; for LAI} < 3 \qquad (3.11)$$

when LAI $\geq$ 3, $\varepsilon_{NB} = 0.98$ and $\varepsilon_o = 0.98$.

For water; $\varepsilon_{NB} = 0.99$ and $\varepsilon_o = 0.985$.

3.5.4 Land Surface Temperature

Land Surface Temperature (T_s) is the temperature of earth's surface as measured using Landsat thermal band (band 6 in Landsat TM and band 10, 11 in Landsat 8). Since band 11 in Landsat 8 encountered large calibration errors than band 10 according to Landsat team (USGS, 2014), band 10 was used for temperature derivation. It was calculated as follows;

$$T_s = \frac{K_2}{\ln(\frac{\varepsilon_{NB} \times K_1}{L_t} + 1)}$$ (3.12)

where;

- L_t is the spectral radiance of thermal band
- K_1 and K_2 are constants for Landsat images from metadata

This surface temperature is irrespective of the elevation due to which higher areas appear cooler. So a topographic adjustment was made to surface temperature according to the lapse rate using DEM;

$$T_{s\_datum} = T_s + 0.0065 \times (DEM\text{-}Elevation\ of\ datum)$$ (3.13)

3.6 Land Use Land Cover Classification

Land use land cover (LULC) classification involves assigning pixels to the information classes which informs about the use of land. Land cover and land use tell what the land surface is covered by and how the land is used for example, urban areas, agriculture, specific crops such as wheat, maize etc. Land use classification is an important component of remote sensing and an input to many analyses like change detection, urbanization studies, pattern recognition etc. Classification approaches are basically divided into per-pixel and object based of which per-pixel approach is most common.

In this study, a per pixel classification method ISODATA unsupervised classification was used for LULC classification. ISODATA involves combining pixels into spectral clusters with spectrally similar characteristics which are then combined into information classes by users. The LULC classification was performed for the two time periods 1998-2000 and 2009-2013. The NDVI for the two time periods were stacked into two composites representing two time periods. Unsupervised classification algorithm ISODATA was applied on these two composites separately and 25 clusters were formed. These clusters were then grouped into six classes on the basis of crop phenology, crop calendar and temporal profile of NDVI. These classes include;

- Bare Soil/ Urban areas/Water
- Natural Vegetation
- Wheat-Fallow
- Wheat-Maize
- Sugarcane
- Tobacco

Accuracy assessment was performed by taking 300 random sample points and their profiles were studied. Confusion matrix was developed and overall accuracy was calculated. The post classification change detection was adopted to assess the changes over the two time periods using change matrix.

3.7 METRIC Model

METRIC model is a surface energy balance based model for ET calculation (Allen et al., 2007) with its algorithms principally based upon SEBAL model developed by Bastiaanssen in Netherland (Bastiaanssen et al., 1998; Bastiaanssen, 1998a). It is primarily an image processing based model with inputs of routine

weather measurements like temperature, wind speed, humidity etc. The brief flow chart of estimating ET using METIC is given in Figure 3.4. In METRIC, the ET is calculated as latent energy flux (LE) where;

$$LE = R_n - G - H \qquad (3.14)$$

where;

- LE is the latent heat flux (W/m^2),
- R_n is the net radiation flux at the surface (W/m^2),
- G is the soil heat flux (W/m^2), and
- H is the sensible heat flux to the air (W/m^2).

3.7.1 Net Radiation

Net radiation R_n is the radiation available at the land surface and is calculated as;

$$R_n = R_{S\downarrow} - \alpha\, R_{S\downarrow} + R_{L\downarrow} - R_{L\uparrow} - (1-\varepsilon_o)R_{L\downarrow} \qquad (3.15)$$

where;

- $R_{S\downarrow}$ is the incoming shortwave radiation (W/m^2),
- α is the surface albedo (dimensionless),
- $R_{L\downarrow}$ is the incoming longwave radiation (W/m^2),
- $R_{L\uparrow}$ is the outgoing longwave radiation (W/m^2), and
- ε_o is the surface thermal emissivity (dimensionless).

Incoming shortwave radiation ($R_{S\downarrow}$) is computed using solar incidence angle, earth-sun distance and atmospheric transmissivity as;

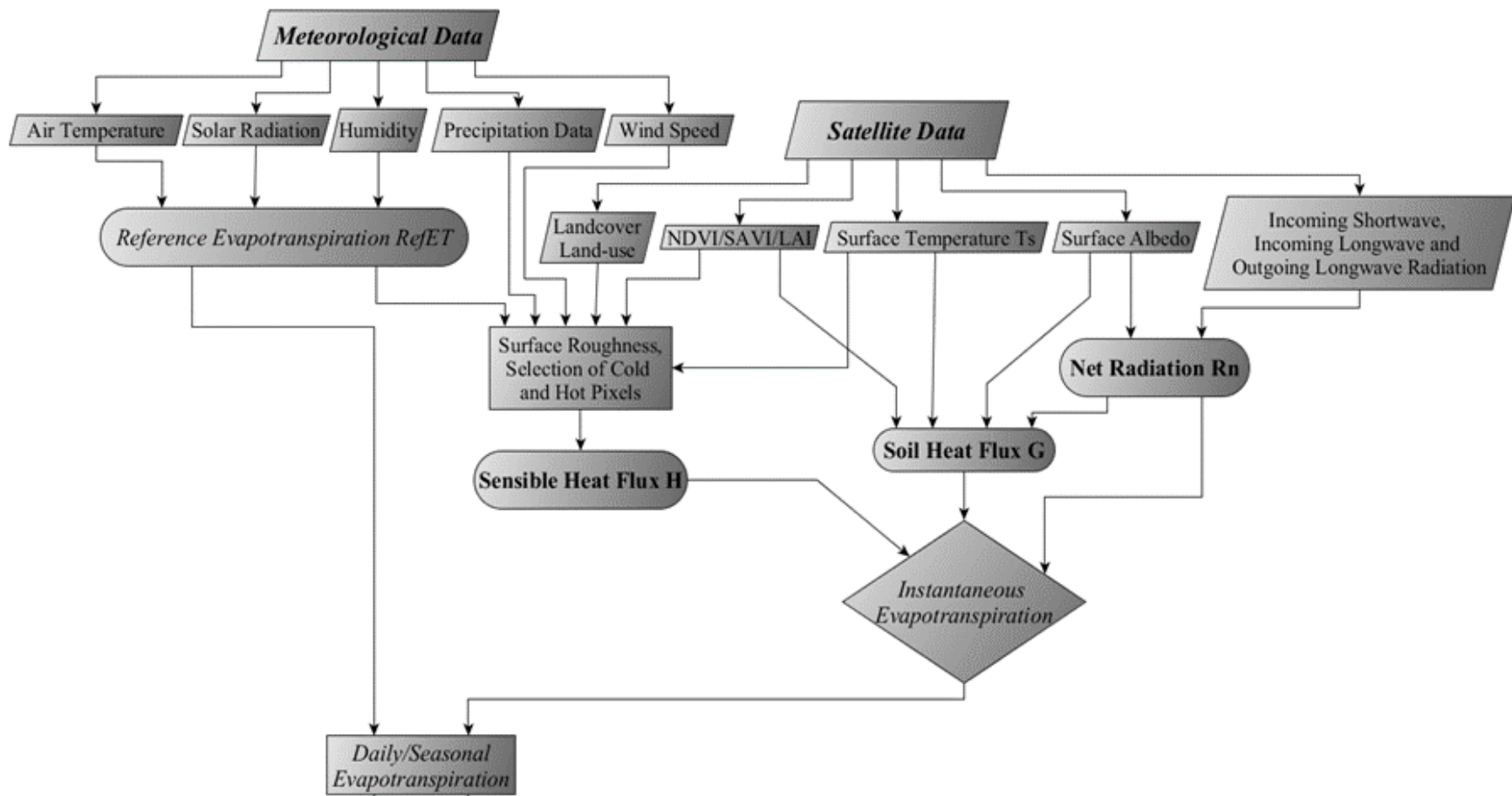$$R_{S\downarrow} = \frac{G_{sc}\cos\theta_{rel}\tau_{sw}}{d^2} \qquad (3.16)$$

Figure 3.4: Methodological flow for estimation of ET using METRIC

Where;

- G_{sc} is solar constant (1367 Wm^{-2}),

- θ_{rel} is solar incidence angle,

- d^2 is square of the relative Earth–Sun distance, and

- τ_{sw} is broad-band atmospheric transmissivity.

    Incoming longwave radiation ($R_{L\downarrow}$) is computed as;

$$R_{L\downarrow} = \varepsilon_a \sigma T_{cold}{}^4 \tag{3.17}$$

where;

- ε_a is effective atmospheric emissivity,

- σ is the Stephen Boltzmann constant (5.678×10-8 W m-2 K-4). and

- T_{cold} is the surface temperature of cold pixel selected adjusted for lapse effect using Eq 3.13.

    Outgoing Longwave Radiation ($R_{L\uparrow}$) is computed as;

$$R_{L\uparrow} = \varepsilon_o \sigma T_s{}^4 \tag{3.18}$$

where;

- ε_o is broad-band surface emissivity,

- σ is Stefan–Boltzmann constant 5.67×10^{-8} (Wm^{-2} K^{-4}), and

- T_s is surface temperature (K).

3.7.2 Soil Heat Flux

Soil heat flux (G) is defined as the rate of heat storage in soil and vegetation. It is calculated as;

$$\frac{G}{Rn} = (T_s\text{-}273.15)(0.0038+0.0074\alpha)(1\text{-}0.98NDVI^4) \tag{3.19}$$

where;

- T_s is the surface temperature (K), and

- α is the surface albedo.

G is then readily calculated by multiplying G/Rn by the value of Rn computed in Eq 3.15.

3.7.3 Sensible Heat Flux

Sensible heat flux (H) is basically the rate of heat lost to atmosphere by convection and advection. It needs careful consideration of ground conditions, land use and require ground observations of wind speed, precipitation and air temperature. It is also complex and involve knowledge of area. It is calculated as;

$$H = \rho_{air} C_p \frac{dT}{r_{ah}} \qquad (3.20)$$

where;

- ρ_{air} is air density (kg/m^3),

- c_p is air specific heat (1004 J/kg/K),

- dT (K) is the temperature difference ($T_1 - T_2$) between two heights (z_1 and z_2), and

- r_{ah} is the aerodynamic resistance to heat transport (s/m) between heights (z_1 and z_2).

The computation of r_{ah} and dT requires selection of two anchor pixels 'cold' and 'hot' pixel. The aerodynamic resistance is calculated using wind speed and iterative stability correction based on Monin-Obhukov function L (Allen et al., 1996). The initial r_{ah} calculated is done using neutral atmospheric conditions and after that the stability corrections are done for r_{ah} in every step until the value of H stabilises. It is calculated as;

$$r_{ah} = \frac{\ln(\frac{z_2}{z_1})}{u_* \times k} \qquad (3.21)$$

where

- z_1 and z_2 are heights above the zero-plane displacement of the vegetation where the endpoints of dT are defined,

- u* is friction velocity (m s^{-1}), and

- k is von Karman's constant (0.41).

This aerodynamic resistance is based on neutral stable atmospheric conditions where friction velocity is computed as;

$$u_* = \frac{ku_x}{\ln(\frac{z_x}{z_{om}})} \qquad (3.22)$$

Where

- u_x is wind speed (m s^{-1}) at a blending height z_x (first calculated as constant for z=200 m as constant for neutral conditions), and

- z_{om} is momentum roughness length (m). (A measure of the friction for the layer of air that interacts with the surface calculated as $0.018 \times LAI$ in agricultural areas).

Another variable needed for calculation of H is dT the near surface temperature difference between heights z_1 and z_2 which is estimated as linear function of T_s as;

$$dT = a\ T_{s\_datum} + b \qquad (3.23)$$

where;

- a and b are empirically determined constants, and

- T_{s_datum} is topographically corrected surface temperature.

The constants a and b require the selection of cold and hot pixels, the 'anchor' pixels. Cold pixel represents the well watered agricultural field; whereas, hot pixel represent dry, fallow agricultural field. The cold and hot pixels were selected using an automated calibration procedure Calibration using Inverse Modelling at Extreme Conditions (CIMEC) developed by Allen et al. (2013).

- At the hot pixel, the H is expressed as;

$$H_{hot} = (Rn - G)_{hot} - LE_{hot} \qquad (3.24)$$

where

  o LE_{hot} is the latent residual evaporation at the hot pixel (normally taken as 0 but is checked by running simple water balance equation), and

  o R_n and G are values for the hot pixel.

The dT for hot pixel is calculated as;

$$dT_{hot} = \frac{(R_n - G)r_{ah\ hot}}{\rho_{air\ hot}C_p} \qquad (3.25)$$

where

  o $r_{ah\ hot}$ is r_{ah} computed for the roughness and stability conditions of the hot pixel, and

  o $\rho_{air\ hot}$ is ρ_{air} calculated at the hot pixel.

- At cold pixel H is estimated as;

$$H_{cold} = (R_n - G)_{cold} - LE_{cold} \qquad (3.26)$$

where

LE_{cold} is estimated latent heat flux at the cold pixel taken as 1.05 $ET_r \times \lambda$ (λ is latent heat of vaporization)

The dT for hot pixel is calculated as;

$$dT_{cold} = \frac{H_{cold} r_{ah\,cold}}{\rho_{air\,cold} C_p} \qquad (3.27)$$

where

- ○ $r_{ah\,cold}$ is r_{ah} computed for the roughness and stability conditions of the cold pixel, and

- ○ $\rho_{air\,cold}$ is ρ_{air} calculated at the cold pixel.

In this way dT is computed and constants are calculated using dT and T_s and H is computed for neutral conditions which is then corrected for stability using corrected r_{ah} values in dT calculation of hot and cold pixels until the value of H stabilises.

3.7.4 Calculation of Evapotranspiration

The LE is calculated using eq 14 which is converted to instantaneous ET as;

$$ET_{inst} = 3600 \frac{LE}{\lambda} \qquad (3.28)$$

where

- ET_{inst} is instantaneous ET (mm h^{-1}),

- 3,600 converts from seconds to hours, and

- λ is latent heat of vaporization (J kg^{-1}).

In this study only daily ET_r values were available so instead of 3600 conversion factor 86400 was used and ET for the day was found which was used to derive ET_rF to extrapolate to seasonal ET;

$$ET_rF = \frac{ET_{inst}}{ET_r} \qquad (3.29)$$

Where ET_r is reference ET at time of satellite overpass.

3.7.5 Seasonal Evapotranspiration

Seasonal ET was calculated using ET_rF and ET_r values over the period as;

$$ET_{period} = \sum_{i=m}^{n} [(ET_rF_i)(ET_{r24i})]$$
(3.31)

Where;

- ET_{period} is cumulative ET for a period beginning on day *m* and ending on day *n*,

- ET_rF_i is interpolated ET_rF for day i, and

- ET_{r24i} is 24 h ET_r for day i.

RESULTS AND DISCUSSION

4.1 Land Use Land Cover Classification

The LULC classification was performed with unsupervised ISODATA clustering technique (Figure 4.1). The accuracy assessment was performed and results are shown in Table 4.1. The overall classification accuracy for 1998-2000 and 2009-2013 time periods was achieved as 82 and 79% respectively, whereas, the kappa statistic was achieved as 0.76 and 0.72 respectively. Most of the confusion was observed between natural vegetation, sugarcane and tobacco due to limited spectral range (only red and NIR bands as NDVI) used in classification and similar spectral response between these classes. Sugarcane and natural vegetation both have high NDVI which causes confusion between two classes. Sugarcane and tobacco have similar cropping pattern and growth stages, so the likelihood of spectral confusion increases.

The area is primarily agricultural as two main rivers, Kabul and Swat Rivers run through the basin irrigating a large area. Bare soil/urban areas cover large area in southern portion of basin that comprises of Peshawar and Nowshera. Peshawar is a metropolitan city which is mostly covered by built-up areas whereas Nowshera is mostly occupied by rock outcrops of Attock Charat range with bare soil and rocks. Charsadda and Mardan districts in north are mostly covered by sugarcane and tobacco, whereas, in Peshawar, most of cultivated area is covered by wheat-maize crops.

Table 4.2 shows the areas of different land use classes in 1998-2000 and 2009-2013. In 1998-2000 (Figure 4.1a), water/bare soil/urban areas covered 26% of the total area, whereas, agricultural land use covered 54% and natural vegetation covered 19% of total area. Among the agricultural land use, wheat-maize was the most abundant covering 27% of the basin and tobacco as next abundant crop covering 16% of basin. In 2009-2013 (Figure 4.1b), water/bare soil/urban areas comprised 30% of the area, whereas, agricultural land use covered 57% of the area and natural vegetation covered 14% of area. Among the agricultural land use, wheat-maize was the most abundant covering 23% of the basin and tobacco covering 20% of basin.

Figure 4.2 show relative areas of land use classes for both time periods. The bare soil/urban areas, sugarcane and tobacco have increased from 1998-2013 whereas, wheat-fallow and wheat-maize cropping area has decreased. The increase in tobacco area can be attributed to its high yield being cash crop and the whole produce has to be bought by the companies as per the policies. Sugarcane area increase can be due to higher prices of sugar over time. The area of wheat-maize decrease can be attributed to shift to other crops and wheat-fallow decrease can be caused due to increase in maize cultivation. Similar trends have been found out by Abid et al., (2014) by analysing crop statistics of Khyber Pakhtunkhwa.
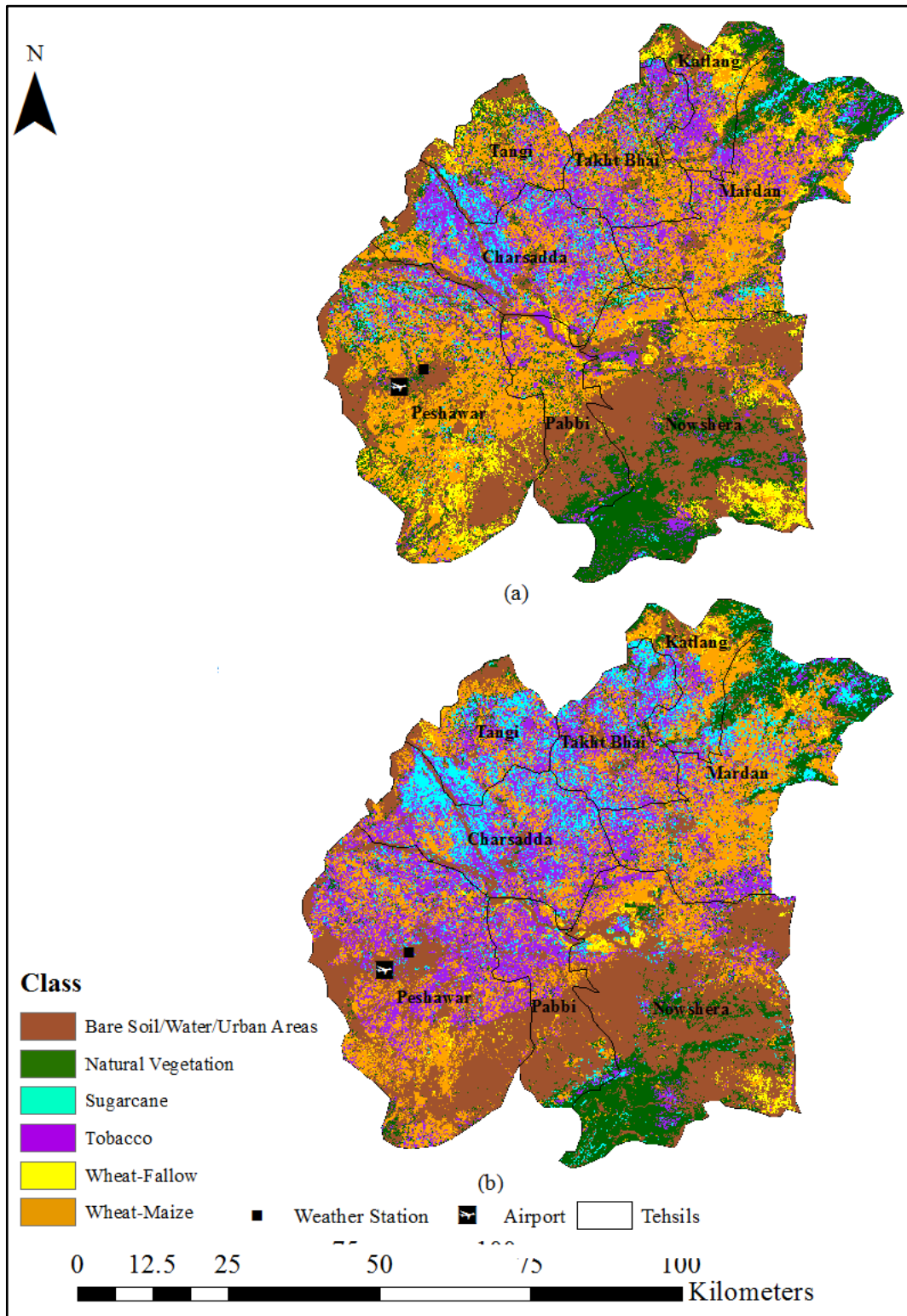
Figure 4.1: LULC classification of (a) 1998-2000 and (b) 2009-2013

Table 4.1: Classification error matrix

(a) 1998-2000									
Classified Data	Reference Data								
	Bare Soil/ Water /Urban Areas	Natural Vegetation	Wheat-Fallow	Wheat-Maize	Sugarcane	Tobacco	**Row Total**	Producer's Accuracy	User's Accuracy
Bare Soil/ Water/ Urban Areas	86	1	1	1	0	0	**89**	87.76%	96.63%
Natural Vegetation	8	31	1	5	4	2	**51**	88.57%	60.78%
Wheat-Fallow	1	1	9	0	0	0	**11**	52.94%	81.82%
Wheat-Maize	1	0	6	77	7	3	**94**	91.67%	81.91%
Sugarcane	0	0	0	0	9	0	**9**	32.14%	100.00%
Tobacco	2	2	0	1	8	33	**46**	86.84%	71.74%
Column Total	**98**	**35**	**17**	**84**	**28**	**38**	**300**		
(b) 2009-2013									
Bare Soil/Water/ Urban Areas	98	2	1	0	0	0	**101**	91.59%	97.03%
Natural Vegetation	2	26	0	3	3	1	**35**	78.79%	74.29%
Wheat-Fallow	0	0	5	2	0	0	**7**	45.45%	71.43%
Wheat-Maize	1	2	5	56	7	4	**75**	90.32%	74.67%
Sugarcane	2	2	0	0	24	6	**34**	48.98%	70.59%
Tobacco	4	1	0	1	15	27	**48**	71.05%	56.25%
Column Total	**107**	**33**	**11**	**62**	**49**	**38**	**300**		

Table 4.2: Areas of LULC classes

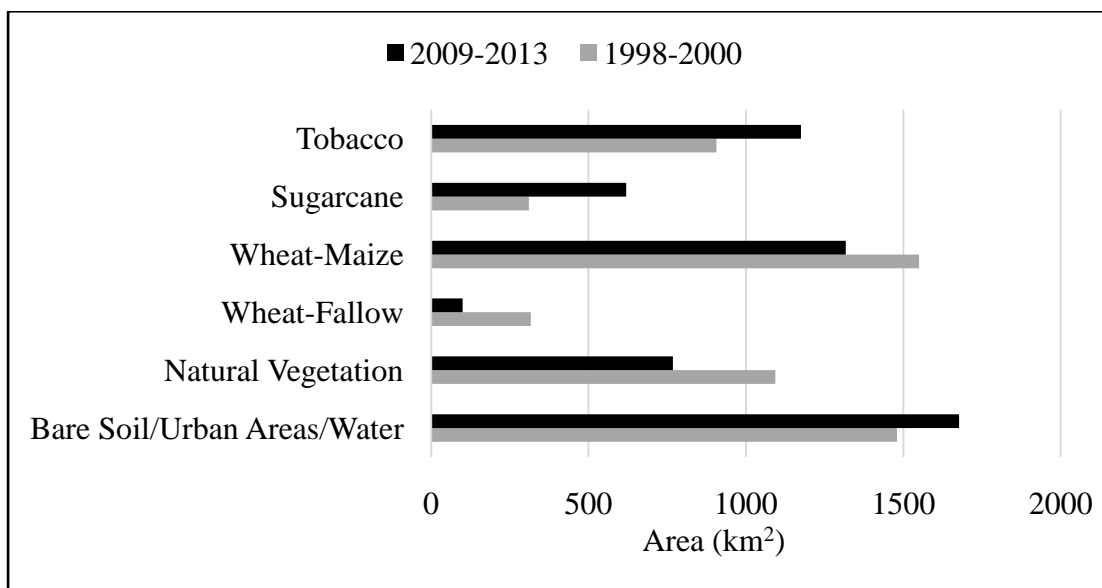| Class Name	1998-2000		2009-2013	
	Area(km^2)	% of total area	Area(km^2)	% of total area
Bare Soil/Urban Areas/Water	1480	26.17	1677	29.64
Natural Vegetation	1094	19.34	768	13.58
Wheat-Fallow	316	5.59	99	1.76
Wheat-Maize	1550	27.40	1318	23.29
Sugarcane	310	5.48	620	10.96
Tobacco	907	16.03	1175	20.77

Figure 4.2: Relative areas of LULC in 1998 and 2013

The post-classification change detection was performed to assess the classes which changed into other classes, and change matrix is given in Table 4.3. The gain in the area of bare soil/urban area/ water class was mostly from the natural vegetation. The area of wheat-fallow class decreased and converted into bare soil or the wheat-maize class whereas, the wheat-maize changed largely into tobacco. The tobacco crop has also gained from sugarcane and natural vegetation. Sugarcane has mostly gained from tobacco.

4.2   Model Validation

The daily actual evapotranspiration values calculated using METRIC were plotted against the reference evapotranspiration ET_r values calculated using FAO-56 Penman Monteith equation (Figure 4.3). Their relationship was explained by linear fit with R^2 value of 0.70 that means that 70% of variation in ET_a is explained by ET_r and there is good correlation between the two. In general, METRIC under-estimated ET_a from March to September (summer) and over-estimated ET_a from October to February (winter). The errors in the estimation can be attributed to the selection of hot and cold pixels affecting calibration and hence accuracy.

Table 4.3: Change matrix of LULC from 1998-2013

From \ To	Bare Soil/ Urban Areas/ Water	Natural Vegetation	Wheat-Fallow	Wheat-Maize	Sugarcane	Tobacco
Bare Soil/ Urban Areas/ Water	-	90	16	50	42	25
Natural Vegetation	203	-	5	148	136	174
Wheat-Fallow	129	14	-	101	6	10
Wheat-Maize	62	107	19	-	119	506
Sugarcane	3	35	0	61	-	137
Tobacco	24	95	3	219	244	-

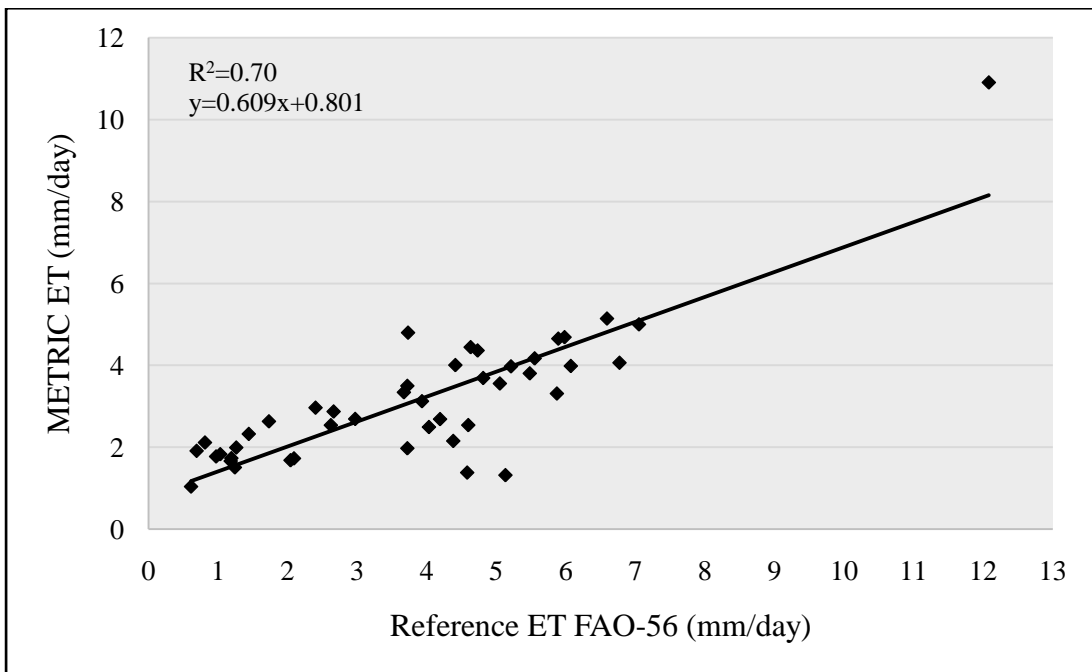Figure 4.3: Comparison of daily ET_a from METRIC with Reference ET

4.3   Spatio-Temporal Patterns of Evapotranspiration

Total of 44 daily ET maps were prepared using METRIC model spanning from 1998-2013. The ET maps show large spatial variations which can be attributed to the wide range of land use, climatic and topographic variations. Most of the ET is affected by the water usage by irrigation through river water and lesser by precipitation as irrigation provides plenty of water to crops in the absence of rainfall, thereby not affecting crop growth.

The results show that the high ET areas lie in the northern part of the basin which comprises Charsadda and Mardan districts. The major reason being that most of the area is covered by agricultural land use composed of sugarcane and tobacco with high water use. Most of the water is provided by Swat River in Charsadda which is the reason of high ET. The low ET areas lie in southern part that comprises Peshawar and Nowshera districts. Major [portion of Peshawar is covered by built-up areas and wheat having low ET. Rock outcrops form major feature of Nowshera district composed of bare soil and natural vegetation due to which ET oscillates between very high and very low ET.

Figures 4.4 – 4.7 show the average daily ET of four seasons of 1998-2000 and 2009-2013. In spring (Figure 4.4), the ET starts increasing as the temperature increases and vegetation growth is at peak especially the wheat crop. In this season, high ET areas are found in northeast Peshawar and upper part of Pabbi Tehsil as these areas are dominated by wheat crop at peak growth. The mean daily ET for the spring season in 1998-2000 is 3.17 mm with a standard deviation (S.D.) of 1.76 mm (Figure 4.4a). In this time period, the ET for agricultural land use range from 2-6 mm. In 2009-2013, ET increased with mean of 3.78 mm/day and

S.D as 1.79 mm (Figure 4.4b). The ET of crops range from 2-8 mm. In Charsadda, the ET is lower as the sugarcane crop is in its early stage of growth. In upper portion of Mardan, ET is higher as this is tobacco growing region which develops from November to August.

In summer (Figure 4.5), ET is at peak because at this time crops are at full growth, temperature is high and there is high precipitation. High ET areas are present around Swat River in Charsadda as in this time of year as sugarcane is at its peak growth and gradually matures which is harvested in September. The mean daily ET in summer of 1998-2000 was 5.23 mm with S.D. of 2.55 mm and the ET of crops range from 4-10 mm (Figure 4.5a). In 2009-2013, the mean ET was 4.39 mm with S.D. of 1.86 mm and ET of crops ranging from 2-8 mm (Figure 4.5b).

In autumn (Figure 4.6) and winter (Figure 4.7), the ET is lowest as the temperature is lowest. In autumn, most of the crops are harvested and the fields are fallow in October and November, and in December, the crops are planted and fields remain bare. The ET is less due to low precipitation resulting in low soil moisture. The mean daily ET of 1998-2000 was 2.30 mm with S.D. 1.58 mm in autumn and 2.48 mm with S.D. 1.25 mm in winter. The ET of crops ranged from 2-4 mm. In 2009-2013 mean daily ET was 2.87 mm with S.D. 1.46 mm in autumn and 2.12 mm with S.D. 1.13 mm in winter. The ET of crops ranged from 2-6 mm.

The ET results show that summer and spring ET has large spatial variations than autumn and winter ET. This is due to larger variations in humidity and precipitation values over the basin.
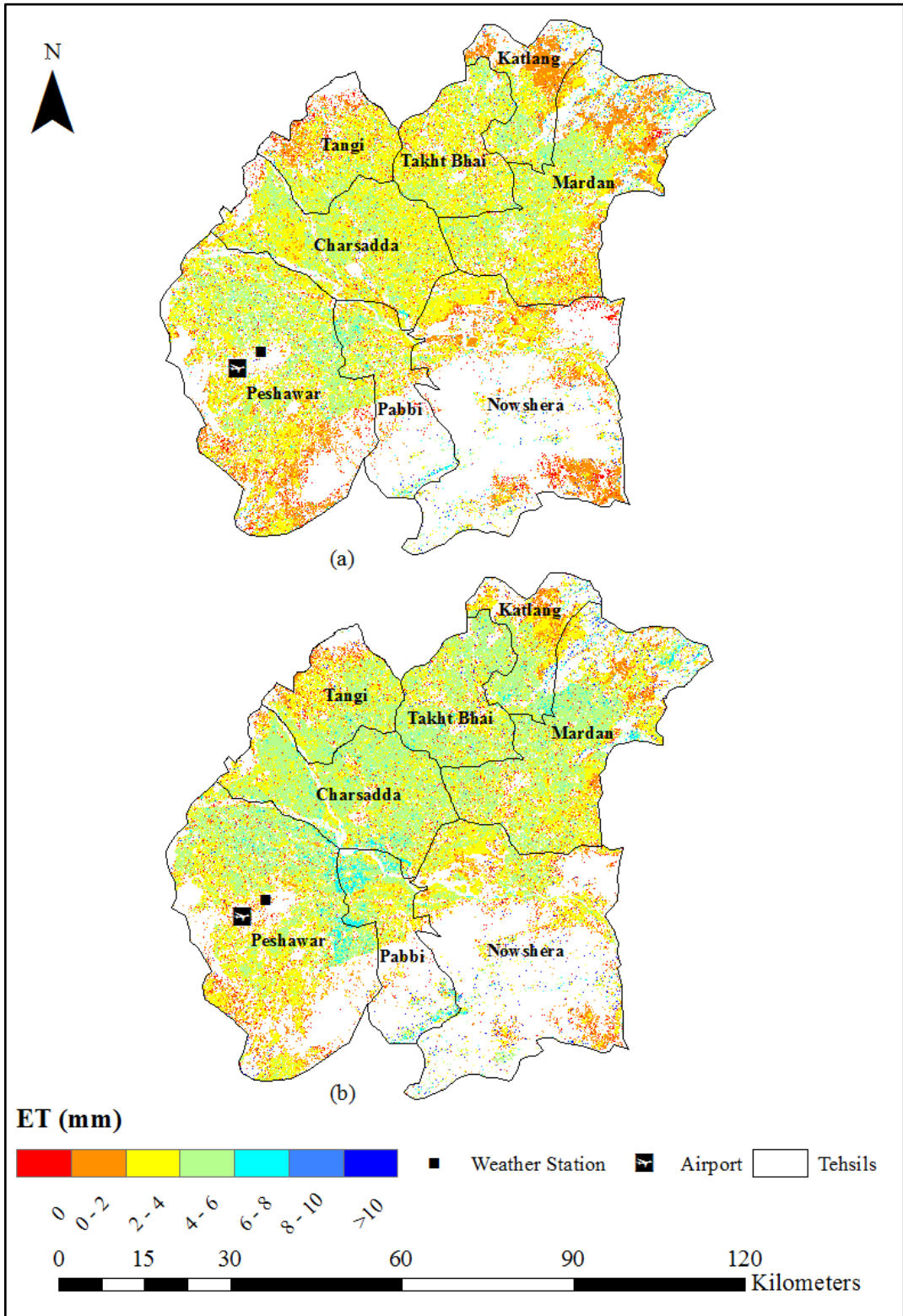
Figure 4.4: Average daily ET in spring (a) 1998-2000 and (b) 2009-2013
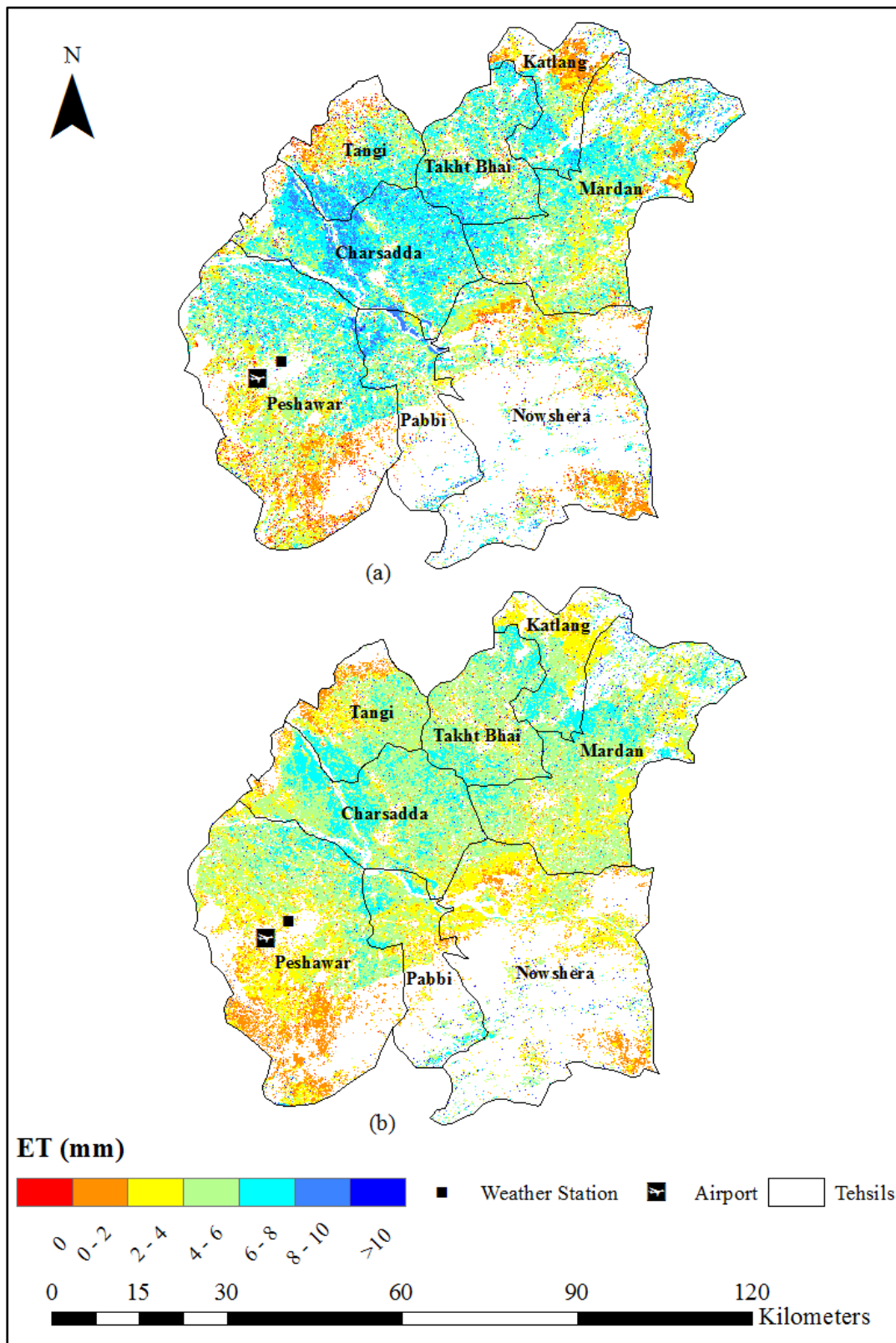
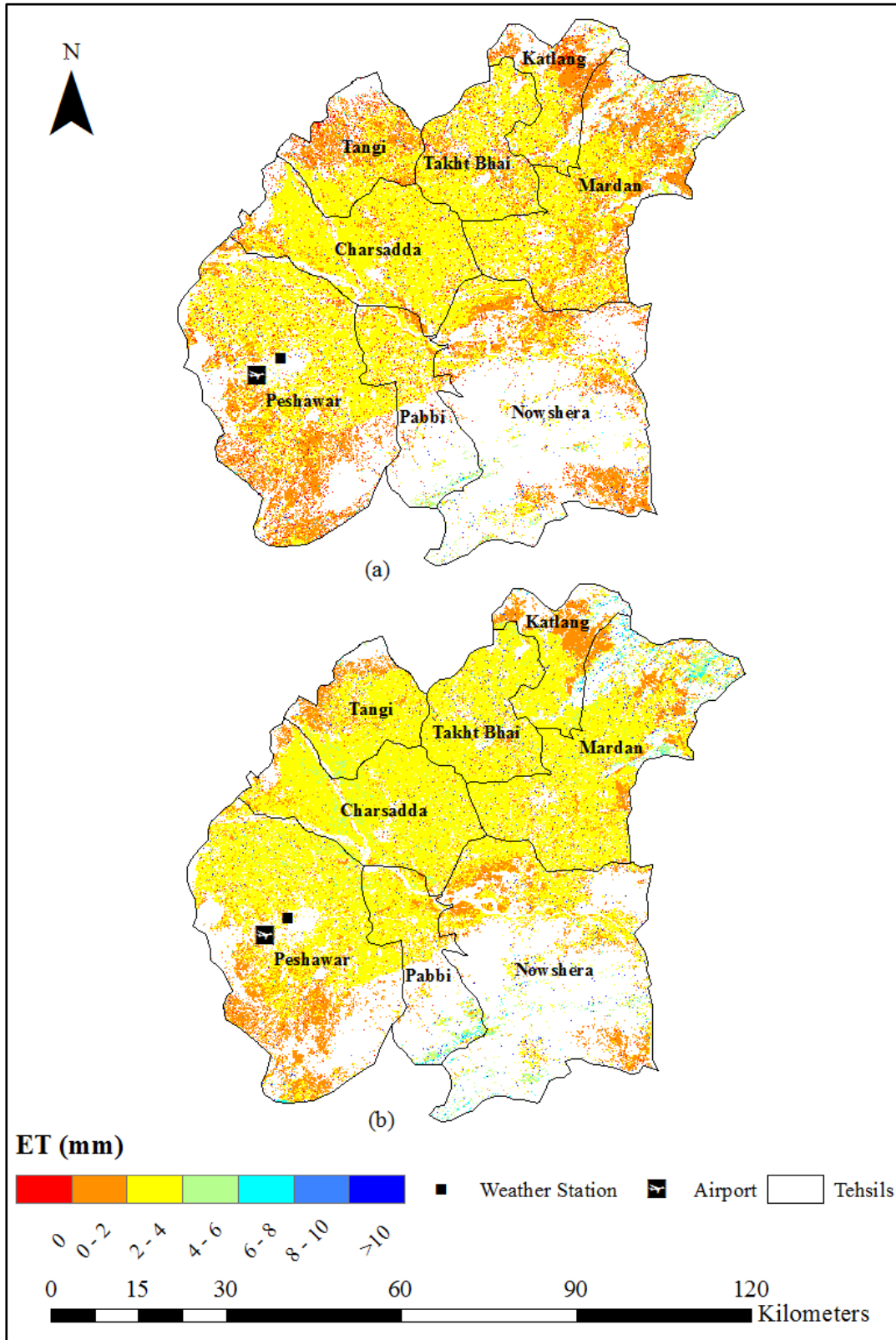Figure 4.5: Average daily ET in summer (a) 1998-2000 and (b) 2009-2013

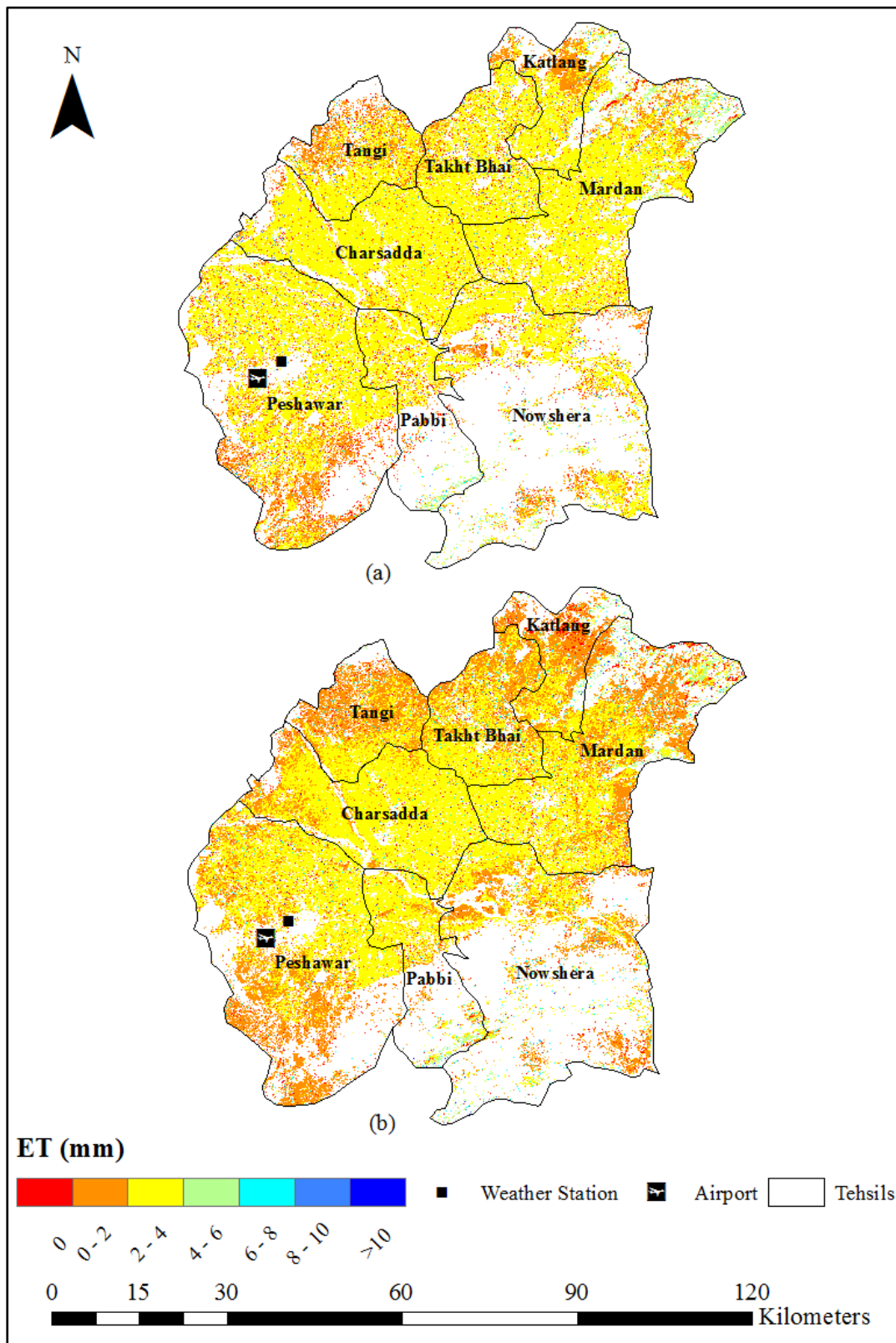Figure 4.6: Average daily ET in autumn (a) 1998-2000 and (b) 2009-2013

Figure 4.7: Average daily ET in winter (a) 1998-2000 and (b) 2009-2013

4.4 Evapotranspiration over Tehsils

The temporal variations in ET were studied by taking tehsils administrative boundaries and overlaying it with daily ET maps (Figure 4.8). For all the tehsils, two peaks have been observed in monsoon season of 1998 and 2009. The detailed analysis revealed that these were the El-Nino years where monsoon rain was in deficit in the basin and temperatures were higher than normal (Rashid, 2004; Shah et al., 2012). This caused the increase in ET higher than normal. Hence, these years were excluded from further analysis to extract temporal trends in ET. Also, tehsils with less agricultural crops were excluded from further analysis (Figure 4.9).

Lowest ET has been observed for Peshawar tehsil due to the large built-up area that has increased over time. The ET range from 1.4 - 4.2 mm. The peak in ET in Peshawar is observed in February to April when wheat is at its peak growth. The ET then decreases and is lowest in December. Another peak is observed in August due to high soil moisture and maize peak growth. The ET of Peshawar has not undergone any significant change from 1998-2013 due to increase in the built-up area over the years that could have balanced any increase in ET for crops.

High ET has been observed for Charsadda, Mardan and Takht Bhai as these tehsils lie in upper portion of the basin receiving high amount of radiations and, have high cultivation of sugarcane and tobacco. The ET in these tehsils range from 2-6 mm, rises from March and reaches at peak in July and August and then decreases to lowest in November and December. The ET in these tehsils has increased over time from 1998-2013 that can be attributed to decrease in humidity. ET in Pabbi tehsil lies in between the ET of Peshawar and Charsadda. Here, the ET ranges from 1.2-5.3 mm and has increasing trend from 1998-2013.

Overall, the ET in tehsils has increasing trend over the years for all of the tehsils (Table 4.4) which can be attributed to increasing temperatures and decreasing humidity and rainfall over time. Although decreasing rainfall decreases soil moisture but as this area is irrigated area and river water is used for cultivation, so the water use does not decrease by decrease in rainfall.

4.5   Evapotranspiration over Agricultural Land Use

Figure 4.10 shows the evapotranspiration for different landuse classes from 1998-2013. Wheat-fallow has the lowest evapotranspiration followed by wheat-maize. Sugarcane and tobacco have highest ET as they have high water consumption.

The evapotranspiration of wheat-fallow follow the growth pattern of wheat crop and range from 0.4 to 3.3 mm. The ET is high in March, April and decrease in May and other months. In June and July, the ET is high due to high soil moisture and temperature. The ET of wheat-maize range from 1.7 to 5.2 mm and follow the pattern of wheat and maize growth. The ET of tobacco and sugarcane are almost same ranging from 2-6 mm. From 1998-2013 the ET of wheat-fallow cropping system has remain unchanged and no significant change has occurred. Wheat-maize has a slight increase in ET from 1998-2013. Significant increase in ET of tobacco and sugarcane has been observed from 1998 -2013.

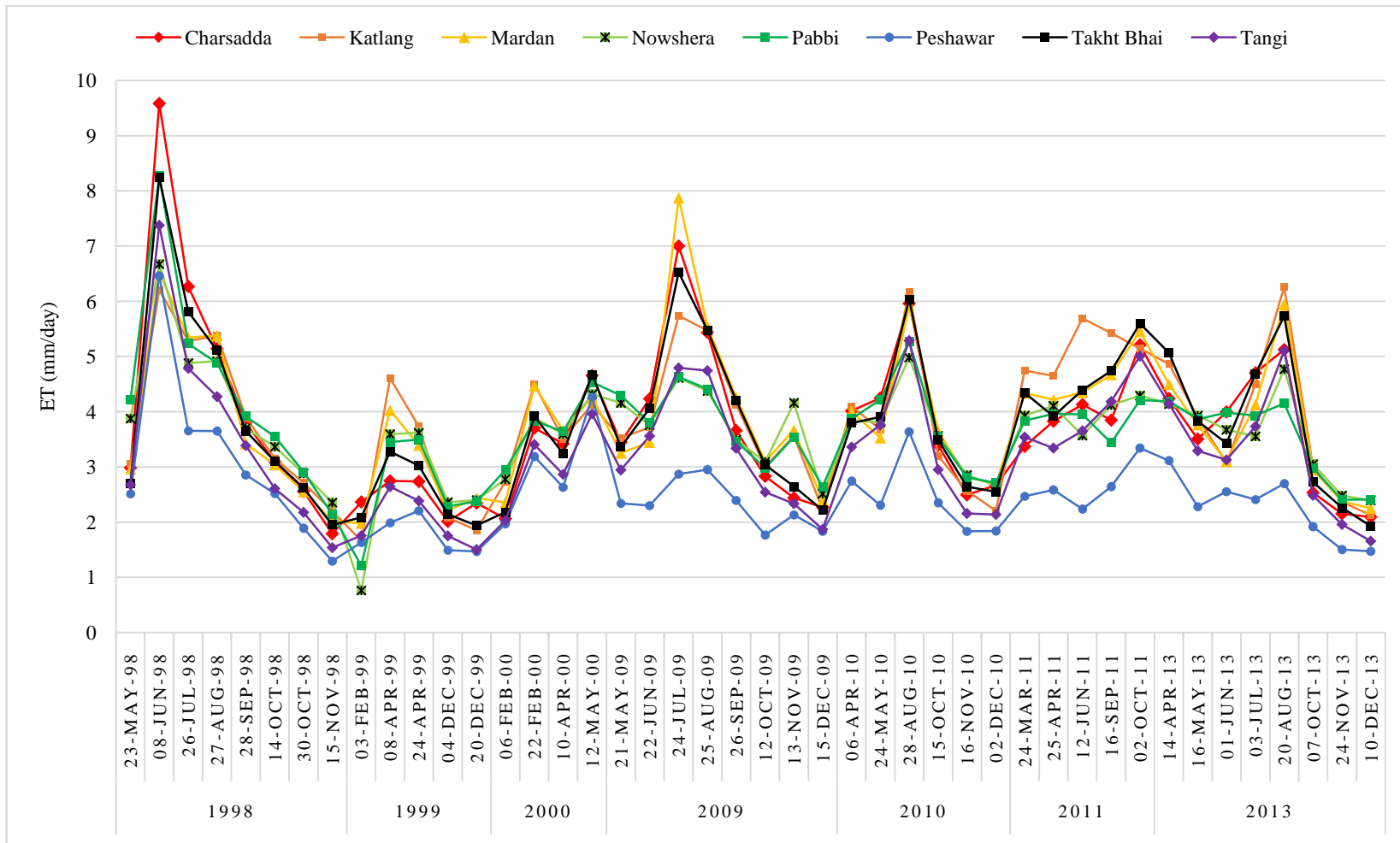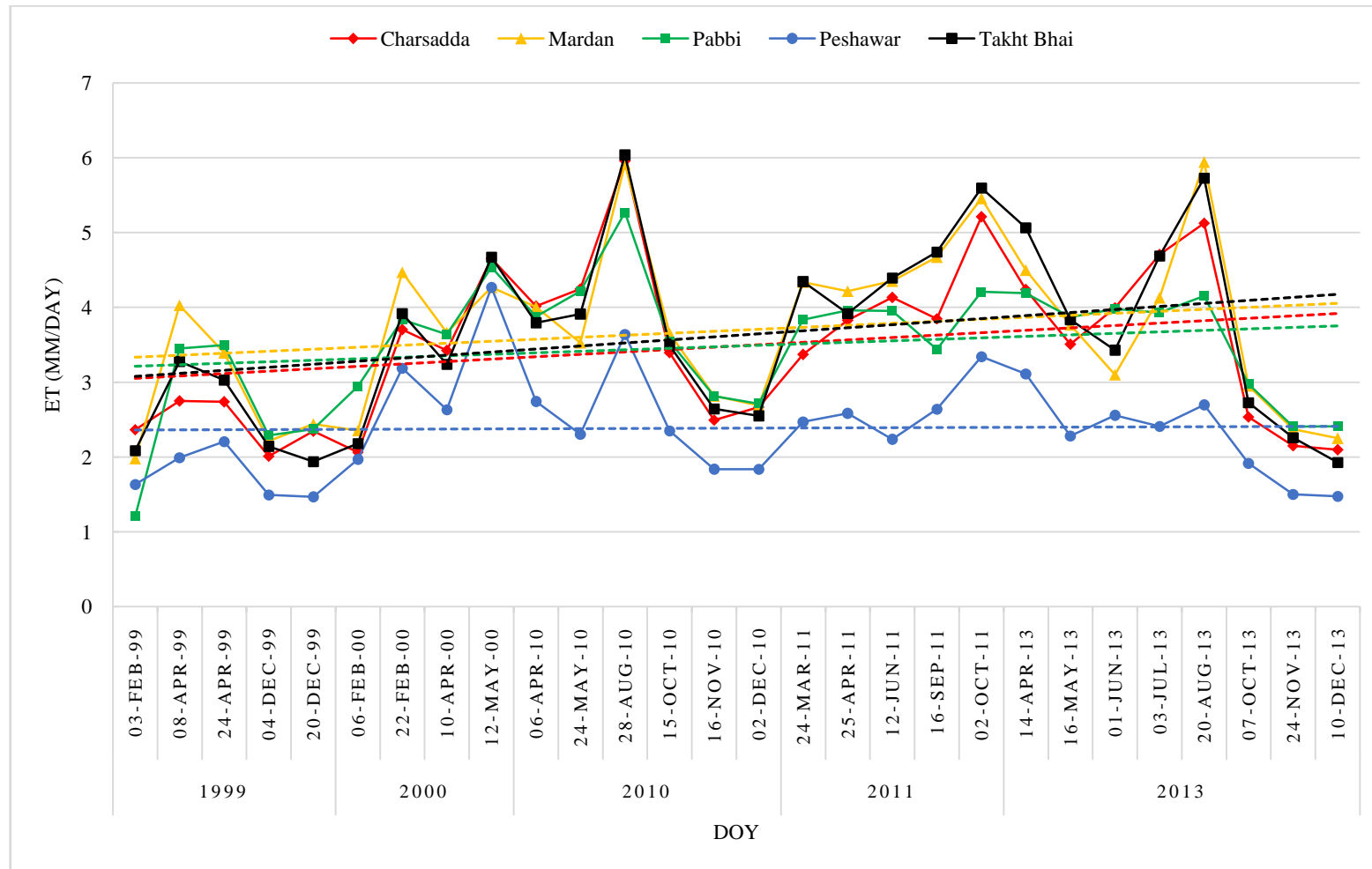Figure 4.8: Temporal pattern of tehsils ET including El-Nino years

Figure 4.9: Temporal pattern of tehsils ET excluding El-Nino years

Table 4.4: Average daily ET of tehsils

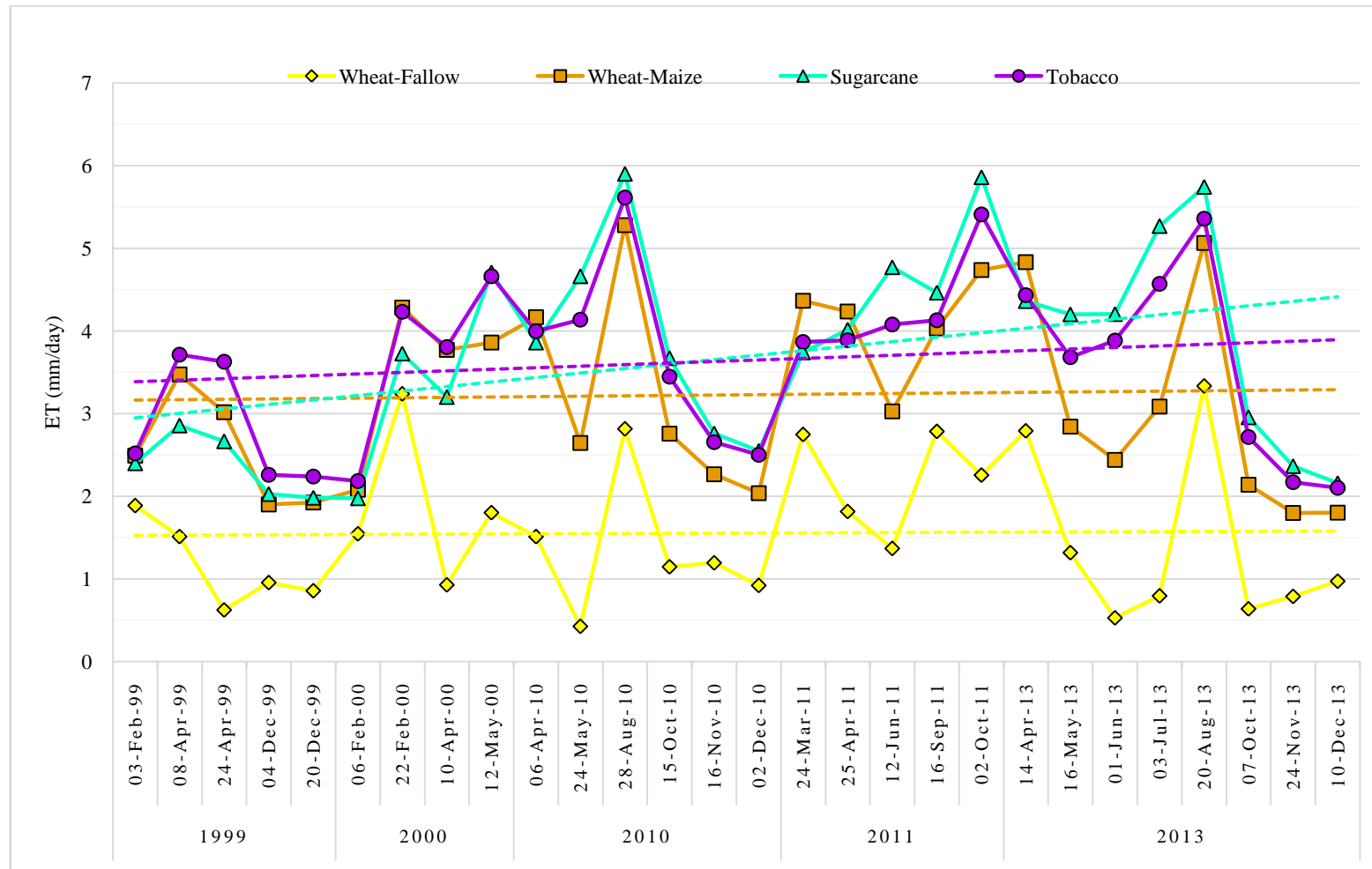| Tehsil	1998-2000 (mm)	2009-2013 (mm)
Charsadda	2.89	3.76
Mardan	3.20	3.93
Pabbi	3.09	3.67
Peshawar	2.32	2.42
Takht Bhai	2.94	3.95

Figure 4.10: Temporal patterns of crops ET from 1998-2013

4.6   Seasonal Evapotranspiration

Seasonal Evapotranspiration was calculated for the Kharif and Rabi seasons for which sufficient number of images were available to accurately extrapolate daily ET. Kharif season spanned from May to October and Rabi season from November to December. Kharif ET was calculated for year 2013 and Rabi ET for years 1999 and 2000 as high cloud cover limited the number of images that could be used.

In 2013, the mean Kharif season ET was 582 mm with agricultural ET ranging between 400-1000 mm (Figure 4.11). The Kharif season ET is higher around rivers where high amount of water is available all season. In rabi season, high ET is around Peshawar and Pabbi due to wheat growth in these areas. In the 1999 rabi season, the mean ET is 292 mm with crops ET ranging from 200-500 mm (Figure 4.12a) whereas, in 2000 rabi season, the ET was higher with mean ET 361 mm and crops ET ranging from 300 mm to higher than 500 mm (Figure 4.12b).
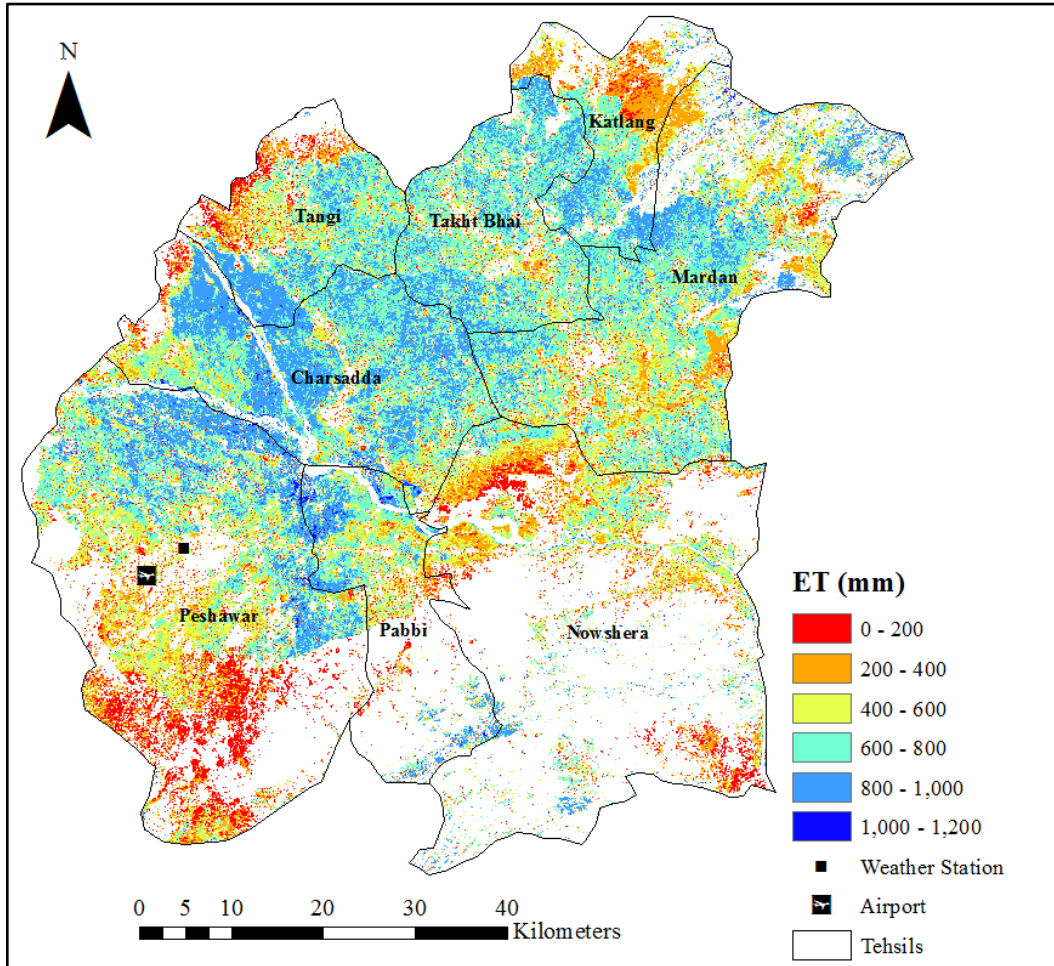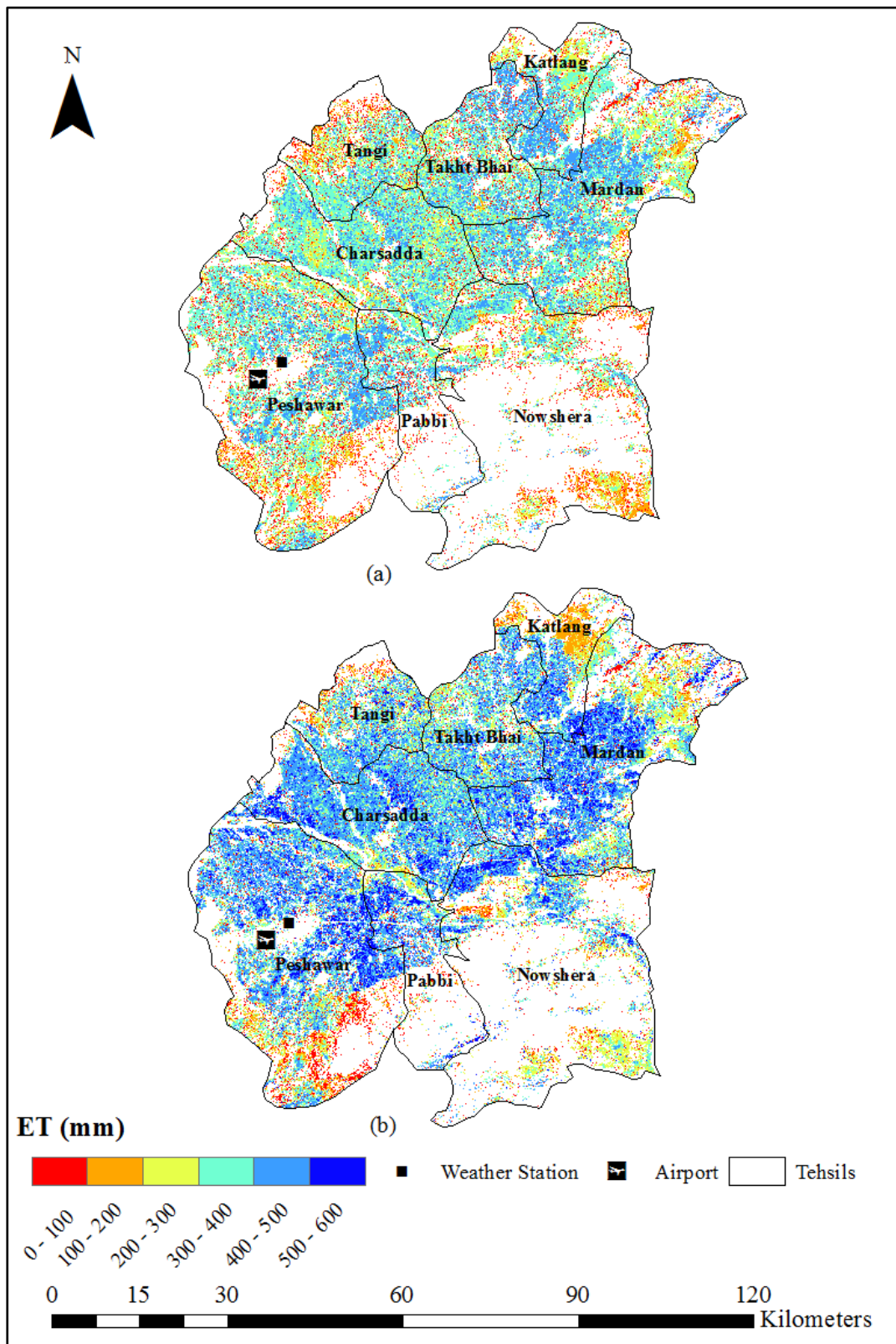
Figure 4.11: Kharif season ET in 2013

Figure 4.12: Rabi season ET (a) 1999 and (b) 2000

4.7   Impact of   Climatic and Biophysical Variables on Evapotranspiration

Linear regression was performed between evapotranspiration and various climatic and biophysical variables recorded and obtained at the Peshawar station to find out the impact of these variables on ET. The regression was carried out only for weather station as the data for climatic varables was only available for weather station and could not be interpolated due to only one point measurement. Climatic variables included minimum temperature, maximum temperature, relative humidity, sunshine hours and wind speed; whereas, biophysical variables included NDVI, T_s and albedo. The scatterplots of these variables against ET with their R^2 values are given in Figure 4.13. The overall R^2 for the combined effect of all variables on ET was found out as 0.68 which shows that 68% variation in ET was explained by these variables.

None of the variable shows very high correlation that shows that one variable cannot explain all of the variation in ET. The variable which has the most impact on ET is temperature as the increase in temperature causes an increased removal of moisture from vegetation. Among temperature variables, minimum temperature has the most influence and represent 62% of variation in ET. Albedo and wind speed are the other two most influential variables. Increase in albedo is due to increased reflectance that increases the net radiation which in turn increases ET. Increase in wind speed helps in transferring the moisture filled air to other places, hence bringing dry air which can absorb more water, thereby increasing ET.
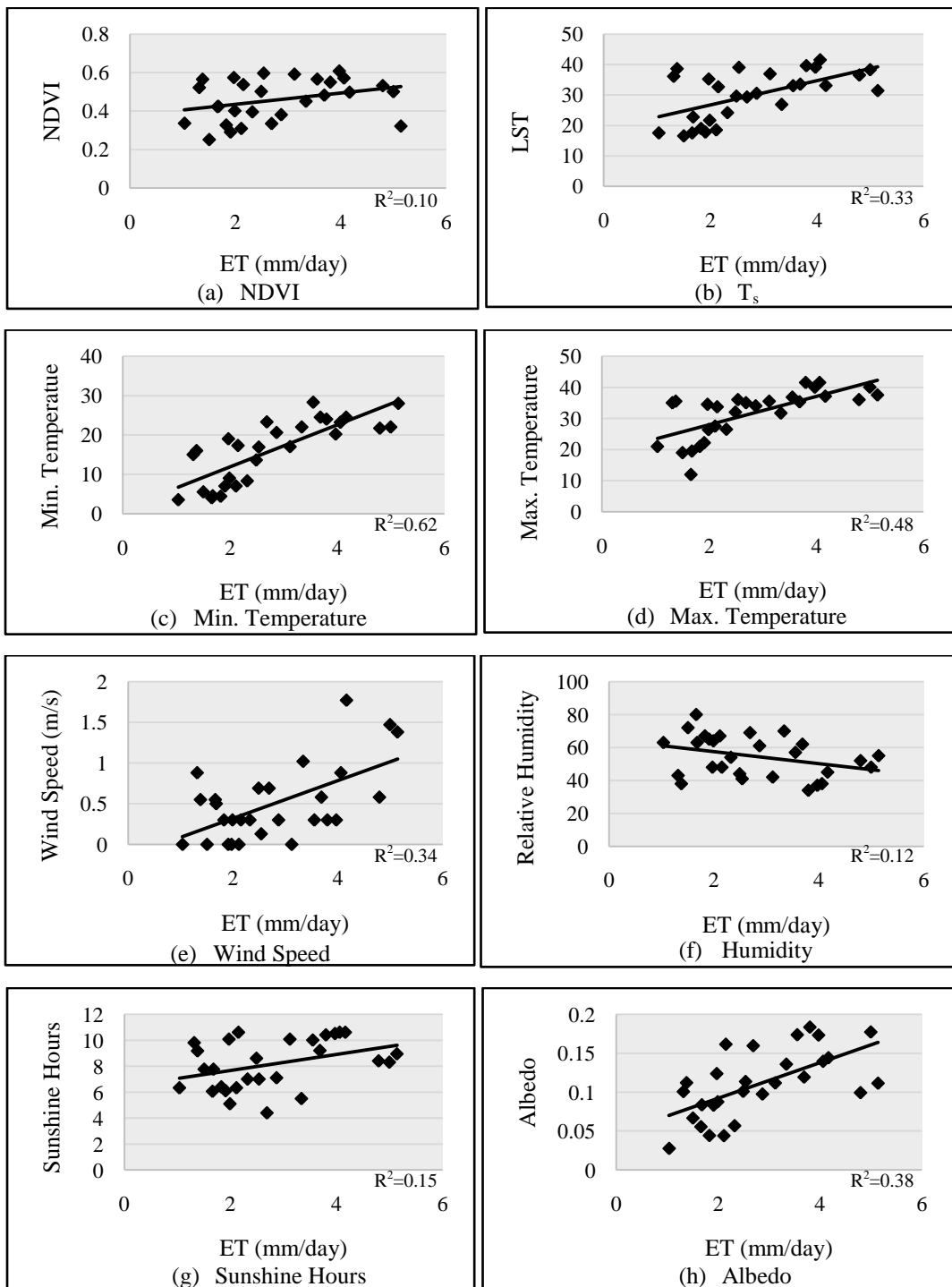
73

Figure 4.13: Relationship of climatic and biophysical variables with ET

CONCLUSIONS AND RECOMMENDATIONS

5.1   Conclusions

In this study, the actual evapotranspiration was estimated using METRIC model employing Landsat 5 TM, Landsat 8 and meteorological data in Peshawar basin for time period 1998-2000 and 2009-2013. The land use land cover classification was carried out for the basin using ISODATA clustering. The model was validated against the reference ET calculated using FAO-56 Penman-Monteith equation. The ET of tehsils were calculated by overlaying tehsils boundary and the ET of agricultural land use was also calculated. The results show that;

1. The land use of area is comprised of wheat, maize, sugarcane, tobacco and bare soil. Wheat-maize comprised most of the area with tobacco next abundant crop. Over the years, sugarcane and tobacco have increased, whereas, wheat-maize cropping decreased.

2. The METRIC model can be well applied to area and the R^2 was found as 0.70.

3. The ET varies with time according to cropping pattern and the climatic variations. ET increases from March and is highest in summers in June and July and then decreases with decrease in temperature and crop harvesting being lowest in winter (December).

4. The ET over Charsadda, Mardan and Takht Bhai is highest ranging from 2 - 6 mm and has increased over time. It is lowest in Peshawar ranging from 1.4 - 4.2 mm but the ET has not changed.

5. The ET of sugarcane and tobacco is highest (2 – 6 mm) with wheat-maize next high (1.7 – 5.2 mm) and lowest for wheat-fallow cropping system (0.4 – 3.3 mm).

6. The ET of Kharif season in 2013 was highest near rivers with mean ET 582 mm. The Rabi ET was highest near Peshawar and Pabbi with mean ET of 292 and 361 mm in 1999 and 2000 respectively.

7. The impact of variables on ET showed that combined R^2 was 0.68 and none of the variables showed strong relation. Only minimum temperature had some good relation with R^2 0.62.

The results showed that the METRIC model can give accurate results for the Peshawar Basin. The Landsat data allowed to study spatial details on field scale which helped in differentiating water use of crops. It is also concluded that the ET in the area has increased from 1998-2013 which shows that more water is being lost by ET. Already, the flow of the Kabul River has decreased over the years and this trend will put further stress on water resources of the area leading to degradation of groundwater also.

5.2   Limitations and Future Research

The major limitation was availability of good weather data which produced errors in estimation of coefficients for sensible heat calculations. Also there were only two weather stations in area from which only one had complete weather data, so computations and calibration were done using data from this weather station. As the climatic conditions ae different in upper part of basin near Mardan, this introduced errors.

Ground calibration of various algorithms for parameters of energy balance like LAI, lapse rate, soil heat flux can help increasing accuracy for which further research is needed. The field measurements using lysimeters or scintillometers at various positions of area can help in detailed validation of data as compared to validation with weather station data which are limited in number.

The impact of climatic and other variables also need to be studied in detail. This can be accomplished by taking historical archives of Landsat data from MSS also along with historical data which can give detailed temporal trends in the change of ET. The ET maps can also be studied in relation to precipitation for aridity potential of area to understand food security issues.

5.3 Recommendations

The ET maps can help the water resource managers in monitoring water use and can help in irrigation management and water losses can be reduced. These maps can be further used in hydrological models to calculate water balance. The tehsils wise ET maps can help town planners in assessing water use and devising strategies to reduce water loss.

REFERENCES

Abid, S., Shah, N. A., Hassan, A., Farooq, A., and Masood, M. A. (2014). Growth and Trend in Area, Production and Yield of Major Crops of Khyber Pakhtunkhwa, Pakistan. *Asian Journal of Agriculture and Rural Development*, *4*, 149-155.

Ahmad, M.-D., Biggs, T., Turral, H., and Scott, C. A. (2006). Application of SEBAL approach and MODIS time-series to map vegetation water use patterns in the data scarce Krishna river basin of India. *Water Science & Technology*, *53*(10), 83-90.

Ahmad, M.-D., Magagula, T. F., Love, D., Kongo, V., Mul, M. L., and Kinoti, J. (2005). Estimating actual evapotranspiration through remote sensing techniques to improve agricultural water management: a case study in the transboundary Olifants catchment in the Limpopo basin, South Africa. In *6th WaterNet/WARFSA/GWP Annual Symposium* (pp. 1–19). Ezulwini, Swaziland.

Al-Kaisi, M. (2000). Crop water use or evapotranspiration. *Integrated Crop Management*, 484(11).

Allen, R. G. (2006). Benefits from tying satellite-based energy balance to reference evapotranspiration. *American Institute of Physics Conference Proceedings, 852*, 127–137. doi: 10.1063/1.2349336

Allen, R. G., Burnett, B., Kramber, W., Huntington, J., Kjaersgaard, J., Kilic, A., … Trezza, R. (2013). Automated Calibration of the METRIC-Landsat Evapotranspiration Process. *JAWRA Journal of the American Water Resources Association*, *49*(3), 563–576. doi:10.1111/jawr.12056

Allen, R. G., et al. 1996. Chap. 4 "Evaporation and transpiration." In Wootton et al., eds., ASCE handbook of hydrology (pp. 125–252). ASCE, Reston, Va.,.

Allen, R. G., Pereira, L. S., Raes, D., and Smith, M. (1998). *FAO Irrigation and drainage paper No. 56*. Rome: Food and Agriculture Organization of the United Nations, 26–40. http://www.kimberly.uidaho.edu/water/fao56/fao56. pdf

Allen, R.G., Tasumi, M., and Trezza, R. (2007). Satellite-based energy balance for mapping evapotranspiration with internalized calibration (METRIC)—Model. *ASCE J. Irrig. Drain. Eng*., *33*, 380–394.

Anderson, M. C., Allen, R. G., Morse, A., and Kustas, W. P. (2012). Use of Landsat thermal imagery in monitoring evapotranspiration and managing water resources. *Remote Sensing of Environment*, *122*, 50–65.

Bastiaanssen, W. G. M. (1998a). The surface energy balance algorithm for land (SEBAL). 2: Validation. *J. Hydrol.*, *212-213*, 213–229.

Bastiaanssen, W. G. M. (1998b). *Remote sensing in water resources management: The state of the art*. Colombo, Sri Lanka: International Water Management Institute,

Bastiaanssen, W. G. M., Ahmad, M.-D., and Chemin, Y. (2002). Satellite surveillance of evaporative depletion across the Indus Basin: evaporative depletion across the Indus Basin. *Water Resources Research*, *38*(12), 9–1–9–9. doi:10.1029/2001WR000386

Bastiaanssen, W. G. M., Menenti, M., Feddes, R. A., and Holtslag, A. A.M. (1998). A remote sensing surface energy balance algorithm for land (SEBAL): 1. Formulation. *J. Hydrol.*, *212–213*, 198–212.

Bastiaanssen, W. G. M., Noordman, E. J. M., Pelgrum, H., Davids, G., Thoreson, B. P., and Allen, R. G. (2005). SEBAL Model with Remotely Sensed Data to Improve Water-Resources Management under Actual Field Conditions. *Journal of Irrigation and Drainage Engineering*, *131*(1), 85–93.

Bawazir, A. S., Samani, Z., Bleiweiss, M., Skaggs, R. and Schmugge, T. (2009). Using ASTER satellite data to calculate riparian evapotranspiration in the Middle Rio Grande, New Mexico, *International Journal of Remote Sensing*, *30*(21), 5593-5603.

Brown, P. (2014). Basics of evaporation and evapotranspiration. Retrieved from http://arizona.openrepository.com/arizona/handle/10150/311700

Chávez, J. L., Gowda, P. H., Howell, T. A., Garcia, L. A., Copeland, K. S., & Neale, C. M. U. (2011). ET mapping with high-resolution airborne remote sensing data in an advective semiarid environment. *Journal of Irrigation and Drainage Engineering*, *138*(5), 416–423.

Choragudi, V.N.R.K. (2011). *Sensitivity Analysis on Mapping EvapoTranspiration at High Resolution Using Internal Calibration (METRIC).* MS Thesis, University of Nebraska-Lincoln, Nebraska.

Dodds, P. E., Barton, A., & Meyer, W. S. (2005). *Review of Methods to Estimate Irrigated Reference Crop Evapotranspiration Across Australia* (No. 04/05). CRC for irrigation Futures. Retrieved from

http://www.clw.csiro.au/publications/consultancy/2005/CRCIFtr04-05-
CropEvapotranspiration.pdf.

Du, J., Song, K., Wang, Z., Zhang, B., and Liu, D. (2013). Evapotranspiration estimation based on MODIS products and surface energy balance algorithms for land (SEBAL) model in Sanjiang Plain, Northeast China. *Chinese Geographical Science*, *23*(1), 73–91.

Ershadi, A., McCabe, M. F., Evans, J. P., and Walker, J. P. (2013). Effects of spatial aggregation on the multi-scale estimation of evapotranspiration. *Remote Sensing of Environment*, *131*, 51–62. doi:10.1016/j.rse.2012.12.007

Ershadi, A., McCabe, M. F., Evans, J. P., and Walker, J. P. (2013). Effects of spatial aggregation on the multi-scale estimation of evapotranspiration. *Remote Sensing of Environment*, *131*, 51–62. doi:10.1016/j.rse.2012.12.007

FAO. (2011). Indus river basin. FAO.

Farg, E., Arafat, S. M., Abd El-Wahed, M. S., and EL-Gindy, A. M. (2012). Estimation of Evapotranspiration ET_c and Crop Coefficient K_c of Wheat, in south Nile Delta of Egypt Using integrated FAO-56 approach and remote sensing data. *The Egyptian Journal of Remote Sensing and Space Science*, *15*(1), 83–89. doi:10.1016/j.ejrs.2012.02.001

Fischer, G., Tubiello, H., Veithuizen, V., and Wiberg, D. (2006). Climate change impacts on irrigation water requirements: global and regional effects of mitigation, 1990-2080. *Tec. Forecasting Soc. Ch., 74,* 1083-1107.

Fisher, J. B., Tu, K. P., and Baldocchi, D. D. (2008). Global estimates of the land–atmosphere water flux based on monthly AVHRR and ISLSCP-II data,

validated at 16 FLUXNET sites. *Remote Sensing of Environment*, *112*(3), 901–919.

Glenn, E.P., Huete, A.R., Nagler, P.L., Hirschboeck, K.K. and Brown, P. (2007). Integrating Remote Sensing and Ground Methods to Estimate Evapotranspiration, *Critical Reviews in Plant Sciences*, *26*(3), 139-168.

Gowda, P. H., Howell, T. A., and Allen, R. G. (2008). *Deriving Hourly Surface Energy Fluxes and ET from Landsat Thematic Mapper Data Using METRICTM.* Paper presented at Pecora 17—The Future of Land Imaging… Going Operational, Denver, Colorado. Retrieved from http://www.asprs.org/a/publications/proceedings/pecora17/0017.pdf

Hadjimitsis, D. G., & Papadavid, G. (2013). Remote Sensing for Determining Evapotranspiration and Irrigation Demand for Annual Crops. In Hadjimitsis, D.G. (Ed), Remote Sensing of Environment - Integrated Approaches (pp. 25-55). InTechopen

Hussain, H., Hussain, Z., Sial, M.H., Akram, W. and Farhan, M. F. (2011). Water Balance, Supply and Demand and Irrigation Efficiency of Indus Basin. *Pakistan Economic and Social Review, 49*(1), 13-38

Hussain, S. S., Mudasser, M., Munir, M., & Manzoor, N. (2005). Climate change and variability in mountain regions of Pakistan implications for water and agriculture. *Pakistan Journal of Meteorology*, *2*(4), 75–90.

IUCN. (2010). *Towards Kabul Water Treaty: Managing Shared Water Resources – Policy Issues and Options* (p. 11). Karachi: IUCN Pakistan.

Jin, X. (2009). *Ecohydrology in water-limited environments using quantitative remote sensing: the Heihe River basin (China) case*. Doctoral Dissertation, Wageningen University, Wageningen, the Netherlands.

Khyber Pakhtunkhwa Development Statistics, (2010). Bureau of Statistics, planning and development department, Government of Khyber Pakhtunkhwa.

Kite, G. W., and Droogers, P. (2000). Comparing estimates of actual evapotranspiration from satellites, hydrological models, and field data: A case study from Western Turkey (Research Report No. 42). Colombo, Srilanka: International Water Management Institute (IWMI).

Kustas, W. (2004). Effects of remote sensing pixel resolution on modeled energy flux variability of croplands in Iowa. *Remote Sensing of Environment*, *92*(4), 535–547.

Li, X., Lu, L., Yang, W., and Cheng, G. (2012). Estimation of evapotranspiration in an arid region by remote sensing—A case study in the middle reaches of the Heihe River Basin. *International Journal of Applied Earth Observation and Geoinformation*, *17*, 85–93.

Li, Z., Liu, X., Ma, T., Kejia, D., Zhou, Q., Yao, B., and Niu, T. (2013). Retrieval of the surface evapotranspiration patterns in the alpine grassland–wetland ecosystem applying SEBAL model in the source region of the Yellow River, China. *Ecological Modelling*, *270*, 64–75.

Maeda, E. E., Wiberg, D. A., and Pellikka, P. K. E. (2011). Estimating reference evapotranspiration using remote sensing and empirical models in a region

with limited ground data availability in Kenya. *Applied Geography*, *31*(1), 251–258.

McCabe, M. F., and Wood, E. F. (2006). Scale influences on the remote estimation of evapotranspiration using multiple satellite sensors. *Remote Sensing of Environment*, *105*(4), 271–285. doi:10.1016/j.rse.2006.07.006

Mkhwanazi, M. M., and Chávez, J. L. (2013). Mapping Evapotranspiration with the Remote Sensing ET algorithms METRIC and SEBAL under advective and non-advective conditions: Accuracy determination with weighing lysimeters, *Hydrology Days*, 67–72.

Mkhwanazi, M., and Chávez, J. L. (2012). Using METRIC to Estimate Surface Energy Fluxes over an Alfalfa Field in Eastern Colorado, *Hydrology Days*, 90–98.

Mkhwanazi, M., Chávez, J. L., and Rambikur, E. H. (2012). Comparison of Large Aperture Scintillometer and Satellite-based Energy Balance Models in Sensible Heat Flux and Crop Evapotranspiration Determination. *International Journal of Remote Sensing Applications*, *2*(1), 25-30. Retrieved from http://www.ijrsa.org/paperInfo.aspx?ID=4688

Mokhtari, M. H., Ahmad, B., Hoveidi, H., and Busu, I. (2013). Sensitivity Analysis of METRIC–Based Evapotranspiration Algorithm. *International Journal of Environmental Research*, *7*(2), 407–422.

Mu, Q., Zhao, M. and Running, S.W. (2011). Improvements to a MODIS global terrestrial evapotranspiration algorithm. *Remote Sensing of Environment*, *115*, 1781-1800.

Mutiga, J. K., Su, Z., and Woldai, T. (2010). Using satellite remote sensing to assess evapotranspiration: Case study of the upper Ewaso Ng'iro North Basin, Kenya. *International Journal of Applied Earth Observation and Geoinformation*, *12*, S100–S108.

Nagler, P., Glenn, E., Nguyen, U., Scott, R., and Doody, T. (2013). Estimating Riparian and Agricultural Actual Evapotranspiration by Reference Evapotranspiration and MODIS Enhanced Vegetation Index. *Remote Sensing*, *5*(8), 3849–3871. doi:10.3390/rs5083849

Nagler, P., Scott, R., Westenburg, C., Cleverly, J., Glenn, E., and Huete, A. (2005). Evapotranspiration on western U.S. rivers estimated using the Enhanced Vegetation Index from MODIS and data from eddy covariance and Bowen ratio flux towers. *Remote Sensing of Environment*, *97*(3), 337–351. doi:10.1016/j.rse.2005.05.011

Nasreen, S. (2006). *Monitoring of Surface water, groundwater, air and soil in Peshawar basin against time the 3rd dimension*. Doctoral Dissertation, University of Peshawar, Peshawar.

Pakistan Bureau of Statistics, GoP. (2010). Pakistan Agricultural Census, 2010.

Penman, H. L. (1948). Natural evaporation from open water, bare soil and grass. *P. Roy. Soc. Lond. A, 193*, 120–145.

Penman, H.L. (1956). Evaporation: An Introductory Survey. *Netherlands Journal of Agricultural Sciences,* 1:9-29.

Priestley, C. H. B. and Taylor, R. J. (1972). On the assessment of surface heat flux and evaporation using large scale parameters, *Mon. Weather Rev.*, *100*, 81–92,

Rana, G., and Katerji, N. (2000). Measurement and estimation of actual evapotranspiration in the field under Mediterranean climate: a review. *European Journal of Agronomy*, *13*(2), 125–153.

Rashid, A. (2004). Impact of El-Nino on summer monsoon rainfall of Pakistan. *Pakistan Journal of Meteorology, 1*(2), 35-43.

Rasul, G. and Mahmood, A. (2009). Performance Evaluation of Different Methods for Estimation of Evapotranspiration in Pakistan's Climate. *Pakistan Journal of Meteorology, 5*(10).

Sarwar, A., and Bill, R. (2007). Mapping evapotranspiration in the Indus Basin using ASTER data. *International Journal of Remote Sensing*, *28*(22), 5037–5046.

Senay, G. B., Budde, M., Verdin, J. P., and Melesse, A. M. (2007). A coupled remote sensing and simplified surface energy balance approach to estimate actual evapotranspiration from irrigated fields. *Sensors*, *7*(6), 979–1000.

Shah, M. A., Zeb, A., and Mahmood, S. (2012). The Rainfall Activity and Temperatures Distribution Over KPK during the Monsoon Season (July to September) 2009. *Pakistan Journal of Meteorology, 8*(16). 43-67

Shuttleworth, W. J. (2008). Evapotranspiration measurement methods. *Southwest Hydrology*, *7*(1), 22–23.

Singh, R. K., Liu, S., Tieszen, L. L., Suyker, A. E., and Verma, S. B. (2012). Estimating seasonal evapotranspiration from temporal satellite images. *Irrigation Science*, *30*(4), 303–313.

Sultan, S., and Ahmad, I. (2008). Determination of Daily Regional Scale Actual Evapotranspiration for Indus Sub-basin using Landsat ETM. *Pakistan Journal of Meteorology, 4*(8), 49-58.

Sun, Z., Wang, Q., Matsushita, B., Fukushima, T., Ouyang, Z., and Watanabe, M. (2009). Development of a Simple Remote Sensing EvapoTranspiration model (Sim-ReSET): Algorithm and model test. *Journal of Hydrology*, *376*(3-4), 476–485. doi:10.1016/j.jhydrol.2009.07.054

Sun, Z., Wei, B., Su, W., Shen, W., Wang, C., You, D., and Liu, Z. (2011). Evapotranspiration estimation based on the SEBAL model in the Nansi Lake Wetland of China. *Mathematical and Computer Modelling*, *54*(3-4), 1086–1092.

Tasumi, M. 2003. *Progress in operational estimation of regional evapotranspiration using satellite imagery.* Doctoral Dissertation, Univ. of Idaho, Idaho.

Tasumi, M., Allen, R. G., and Trezza, R. (2008). Estimation of at-surface reflectance and albedo from satellite for routine, operational calculation of land surface energy balance. *J. Hydrol. Eng*., *13*(2), 51-63.

Teixeira, A. H. de C., Bastiaanssen, W. G. M., Ahmad, M. D., and Bos, M. G. (2009). Reviewing SEBAL input parameters for assessing evapotranspiration and water productivity for the Low-Middle São Francisco River basin, Brazil Part B: Application to the regional scale. *Agricultural and Forest Meteorology*, *149*(3-4), 477–490. doi:10.1016/j.agrformet.2008.09.014

Thoreson, B., Clark, B., Soppe, R., Keller, A., Bastiaanssen, W., and Eckhardt, J. (2009). Comparison of evapotranspiration estimates from remote sensing (SEBAL), water balance, and crop coefficient approaches. *In Proceedings ASCE World Environmental and Water Resources Congress 2009: Great Rivers*, *Kansas City, Missouri*, 4347-4361. Retrieved from http://ascelibrary.org/doi/pdf/10.1061/41036(342)437

Trezza, R., Allen, R., and Tasumi, M. (2013). Estimation of Actual Evapotranspiration along the Middle Rio Grande of New Mexico Using MODIS and Landsat Imagery with the METRIC Model. *Remote Sensing*, *5*(10), 5397–5423. doi:10.3390/rs5105397

Turral, H., Burke, J., and Faurès, J.-M. (2011). *Climate change, water and food security (No. 36).* Rome, Italy: FAO. Retrieved from www.fao.org/docrep/014/i2096e/i2096e.pdf

Ullah, M. K., Habib, Z., and Muhammad, S. (2001). *Spatial distribution of reference and potential evapotranspiration across the Indus Basin Irrigation Systems* (Working Paper No. 24). IWMI.

United States Geological Survey. (2014). Landsat 8 (L8) Operational Land Imager (OLI) and Thermal Infrared Sensor (TIRS): Calibration Notices. Retrieved April 15, 2014 from http://landsat.usgs.gov/calibration_notices.php.

University of Idaho, R. Allen. 2013. REF-ET: Reference Evapotranspiration Calculation Software for FAO and ASCE Standardized Equations. Version 3.1.15 for Windows.

Vinukollu, R. K., Wood, E. F., Ferguson, C. R., and Fisher, J. B. (2011). Global estimates of evapotranspiration for climate studies using multi-sensor

remote sensing data: Evaluation of three process-based approaches. *Remote Sensing of Environment*, *115*(3), 801–823.

www.earthexplorer.usgs.gov

Yang, Y., Shang, S., and Jiang, L. (2012). Remote sensing temporal and spatial patterns of evapotranspiration and the responses to water management in a large irrigation district of North China. *Agricultural and Forest Meteorology*, *164*, 112–122.